Numerical investigations on the tool wear of Single Crystal Diamond tool while Modulation Assisted Machining of hardened steel

By

Shekhar Kumar

ENGG1A201801012

Bhabha Atomic Research Centre

A thesis submitted to the

Board of Studies in Engineering Sciences

In partial fulfillment of requirements
for the Degree of

MASTER OF TECHNOLOGY

of

HOMI BHABHA NATIONAL INSTITUTE

January, 2021

Homi Bhabha National Institute

Recommendations of the Thesis Examining Committee

As members of the Thesis Examining Committee, we recommend that the thesis prepared by "Shekhar Kumar" entitled "Numerical investigations on the tool wear of Single Crystal Diamond tool while Modulation Assisted Machining of hardened steel" be accepted as fulfilling the thesis requirement for the Degree of Master of Technology.

	Name	Signature
Member-1	Dr. M.K. Samal	02.02.2021
Member-2	Dr. D. Mukhopadhyay	2/2/2021
Member-3	Dr. T.A. Dwarakanath	02/02/21
Member-4	Dr. D. K. Chandraker	02.02.2021
Technology Advisor	Shri.A.R.Rakesh	01/02/21
Guide	Dr. R. Balasubramaniam	2/2/21
Chairman	Dr. J. Chattopadhyay	J. Chattopadhyay 2/2/2021

Final approval and acceptance of this thesis is contingent upon the candidate's submission of the final copies of the thesis to HBNI.

I hereby certify that I have read this thesis prepared under my direction and recommend that it may be accepted as fulfilling the thesis requirement.

Date: 2.2.2021

Place: Mumbai

Name of Guide: Dr.R.Balasubramaniam

DECLARATION

I, hereby declare that the investigation presented in the report has been carried out by me. The work is original and has not been submitted earlier as a whole or in part for a degree / diploma at this or any other Institution / University.

SHEKHAR KUMAR

ACKNOWLEDGEMENTS

I would like to express my gratitude to my project guide **Dr R. Balasubramaniam** for his guidance and continuous support during this project work. I would also like to thank my mentor **Dr. James Jacob, Shri. A. S. Patil** and my technical adviser **Shri A. R. Rakesh** for believing in me and giving me opportunity to take up this project and without theirs support and valuable suggestion and feedback it would have been impossible to progress through the project. Sincere thanks are to **Dr. Prabhat Ranjan, Dr. Anuj Sharma** and **Shri Satyam Agrahari** for sharing their valuable time and knowledge with me. I would like to express my sincere gratitude to **Dr. Shashank Shekhar** and **Shri Sanjeev Kumar Patel** from IIT, Kanpur for sharing their practical knowledge and valuable time with me. Thanks to my batch mates for helping me at different juncture of this project.

Table of Contents

List of Figures

List of Tables

List of Abbreviations

AFM	Atomic Force Microscope
DTM	Diamond Turning Machining
DTW	Diamond Tool Wear
EVAM	Elliptical Vibration Assisted Machining
FEM	Finite Element Method
LAMMPS	large Atomic/Molecular Massively Parallel Simulator
MAM	Modulation Assisted Machining
OM	Optical microscope
PCD	Poly Crystal Diamond
SCD	Single Crystal Diamond
SEM	Scanning Electron Microscope
UMR	Unit Material Removal
UPDT	Ultra Precision Diamond Turning
UPM	Ultra Precision Machining
ECM	Elliptical Cutting Machining

Synopsis

Diamond tools are subjected to excessive tool wear when used for the cutting of ferrous materials. The diamond tool wear is chemical in nature and is affected by the tool-workpiece combinations and cutting conditions. Graphitization is considered as main cause for the diamond tool wear. Modulation Assisted Machining (MAM) is one of the methods, used for mitigation of diamond graphitization wear process. To understand the problem, a methodology was developed to calculate the tool tip temperature and cutting forces generated during machining process to achieve the tool wear rate during diamond cutting of hardened steel. A Finite Element Analysis (FEA) model was prepared to simulate the tool wear for single crystal diamond tool. For this tool wear model was given work material- tool combination, numerical simulation was used to find out the temperature at the tool tip. The tool tip temperature values were used with an Arrhenius tool wear model selected from the literature. The wear model was validated with experimental values obtained from literature against tool wear and cutting forces. This validated model was later used for optimization of the cutting parameter during elliptical cutting process. For the parameter optimization process various FEA simulations were conducted with different process parameters like cutting velocity, cutting frequency, amplitude of ellipse etc. The tool wear was calculated for those all cases and the effect of contact time on tool wear was studied.

Chapter 1
Introduction

Diamond Tools are widely used to machine metals, ceramics, plastics, composites etc. The industrial need of miniaturization has also improved Diamond Tools and Ultra Precision Machining (UPM) performance in the fields of optics, biotechnology, medicine, electronics, nuclear and communications. However, in case of conventional-machining of ferrous metals, diamond tools are subjected to high wear which subsequently leads to surface deterioration and rapid tool wear. Thus, the applicability of diamond cutting for the machining of ferrous materials is greatly restricted by the short diamond tool life due to the high tool wear rate. Diamond tool wear can have various wear mechanisms namely adhesive, abrasive, graphitization, diffusion, carbide formation, oxidation wear etc. To mitigate/eradicate the effect of tool wear, especially during machining of ferrous metals, approaches like cryogenic turning, inert gas environment cutting, protective coatings, Modulation Assisted Machining (MAM), ion implantation etc. have been tested. Among these methods, Modulation Assisted Machining has been found to be the most promising technique for industry in terms of economical machine setup and long diamond tool life.

Diamond Tool Wear (DTW) mechanisms, broadly, can be classified into mechanical, physical and chemical wear. Mechanical wear includes abrasive wear, fatigue and adhesive wear generally dominant in case of non-ferrous metal cutting. Physical wear involves thermo-chemical wear, anisotropy and defects in the crystal structure of diamond tool. Chemical wear covers chemical reaction, graphitization, amorphization, and diffusion, which becomes ddominant in case of ferrous metal cutting with diamond tool. With a diamond tool, it is easy to achieve submicron surface roughness while cutting nonferrous materials such as aluminum, copper alloy, electroless nickel, and acrylic plastics. The combination of ultra-precision machine tool and ultra-sharp cutting tools make it possible to remove material from the work piece with very small ‘Unit Material Removal’ (UMR). The ratio of the uncut chip thickness to the cutting-edge radius plays a vital role in UPM. As the UMR is very small in Diamond Turning Machining (DTM), the corresponding uncut chip thickness also becomes very small, typically in the order of few microns.

This necessitates requirement of a Single Crystal Diamond (SCD) tool which can confirm a very sharp cutting edge for a long period of time during machining [1]. A diamond turn machine possesses merits like vibration isolation, constant temperature control, and high stiffness in both radial and axial direction for all axes. Its high sliding accuracy, assembly accuracy, positioning and repositioning accuracy, high precision tool and high servo performance, precise feedback and programming resolution helps it to generate submicron surface roughness [1].

The DTW while cutting a non- ferrous material is generally governed by mechanical-type wear namely abrasive and adhesive wear. Since the hardness of diamond tool is quite high as compare to non-ferrous materials, the mechanical tool wear rate becomes quite low. As a result, diamond tool can last for a cutting distance of a few hundred kilometers during cutting of a non-ferrous material.

During the cutting of ferrous metals with the diamond tool, DTW proves to be an inevitable phenomenon because the normal metal cutting conditions like tool tip temperature and pressure, generally favor the chemical wear of diamond tool. As a result, diamond tools are subjected to high wear within a very short cutting distance, which subsequently downgrades the machined surface quality. For example, the DTW rate in turning of mild steel is 10^4 times faster than in turning brass of comparable hardness. This chemical wear may take place through carbon–oxygen, carbon–metal or metal–carbon–oxygen complexes, graphitization (sp^3 diamond changes into sp^2 graphite form) or diffusion wear (Carbon atoms from diamond diffuse into material vacancies). Graphitization is considered as the precursor of DTW.

DTW is influenced by cutting conditions (mainly temperature) generated at the tip of diamond tool, workpiece material, cutting fluid and the gaseous environment in which metal cutting is performed. The rate of chemical wear is strongly associated with the workpiece material and mainly accelerated by high temperatures and pressures produced at the interface between diamond tool and workpiece. Catalytic action of workpiece, activity of the clean surface and gaseous environment also influence the wear rate. Metals having unpaired d-electrons show high tool wear rate of diamond tools due to their high chemical affinity towards carbon-atoms.

The measurement of DTW can directly be accomplished by optical measurement, Scanning Electron Microscope (SEM), and Atomic Force Microscope (AFM). They are considered as an efficient means to estimate tool wear lands, tool wear features, and tool wear mechanisms. Optical microscope (OM) is the most direct, simplest and convenient method for detecting DTW features through optical amplification.

In MAM, the motion of the tool is modulated by imposing ultrasonic vibrations on the diamond tool machining the workpiece. These modulations/vibrations can be imposed in three different directions namely, principal or cutting direction, thrust direction, and feed direction**.** MAM is an intermittent metal removal technique which ensures the disengagement of tool tip with the workpiece during each cutting cycle. In elliptical-MAM, the modulated tool tip locus (combination of elliptical motion and liner cutting motion) generates the finished surface. During each cycle, in the beginning of cutting tool tip comes into contact with workpiece. The tool vibrated elliptically starts to cut. During tool tip and workpiece contact interval, ultrasonic elliptical vibration cutting takes place. In the end of cutting cycle tool is separated from the workpiece and in the next cycle the same modulated-cutting cycle repeats itself.

MAM helps to suppress DTW, especially chemical wear, during the cutting of ferrous metals. It is theorized that by ensuring low cutting temperature (due to better heat dissipation during disengagement of tool and workpiece) and by reducing contact time between diamond tool and workpiece the rate of chemical wear reduces which in turn reduces DTW.

1.1 Background

There is still a lack of understanding about graphitization, oxidation and diffusion phenomenon in cutting process of ferrous metals; especially in case of hardened steels. In order to better understand the tool wear phenomenon’s, the chemical wear mechanisms are to be researched thoroughly and their comprehensible wear mechanisms are needed to be verified. The effectiveness of the MAM for reducing the tool wear in case of hardened steels is still to be explored to give an accurate prediction of optimum parameters for the cutting process.

1.2 Objective

The objectives of this research work are

- Developing a methodology to calculate the tool tip temperature generated during machining process to achieve the tool wear rate during diamond cutting of hardened steel.
- Developing a FEA model to predict diamond tool wear in elliptical cutting.
- Finding out the effect of contact time on the diamond tool wear in elliptical cutting.

1.3 Scope of work

- Numerical simulation, tool wear calculations and tool wear prediction of single crystal diamond tool while modulation assisted machining of hardened steel.
- Validation of FEA model for tool wear
- Optimization of process parameters.

1.4 Organization of thesis

Chapter-1 gives the background and relevance of this research work and the complexities involved. In Chapter-2, the detailed literature survey was carried out in the areas of interest and identifies the gap areas and the scope of this research work. Chapter-3 gives the details of the Numerical simulation carried out on the given work piece material and tool material to determine the temperature and cutting forces at the tool tip for conventional cutting. The Arrhenius tool wear coefficients are selected from the literature to validate the wear model with the numerical simulation for conventional cutting. This Conventional cutting wear model is further used for elliptical cutting simulations.Chapter-4 provides insights about elliptical cutting process. The FEA modeling of tool tip temperature and cutting forces is conducted for elliptical cutting process. The FEA model for elliptical cutting is validated with literature values on the basis of tool wear and cutting forces. In Chapter-5, the validated FEA model for elliptical cutting and forces is used in this chapter to find a relation between tool wear and contact time. A number of FEA simulations are conducted for better visualization of the effect of contact time on tool wear.Chapter-6 gives the important conclusions form this study and future work that provide the scope for the subsequent research in this field

Chapter 2
Literature survey

2.1 Introduction

Tool wear has large influence on economics of machining operation, also its direct effect can be seen on from accuracy and surface roughness of surface generated. Various factor governs tool wear, thus the knowledge of tool wear mechanism and capability of predicting tool life are important and necessary in metal cutting. Since tool wear in cutting operation involves complex wear mechanism, earlier attempt has been made to directly relate tool life to the applied machining parameters (cutting speed, feed, etc.). Taylor's tool life equation is of this type. Nowadays different models describing the diamond tool wears are proposed. To describe the diamond tool wear phenomena a thorough understanding of different wear mechanism is mandatory. Based on the knowledge of wear mechanism associated with tool and work piece material and range of cutting condition suitable wear rate model can be chosen. Tool wear can be estimated with the help of temperature and stresses on tool tip as predicted by numerical simulation.

2.2 Diamond tool and its characteristics

Generally, diamonds tools are used for cutting ultra-precision components due high surface accuracy and very low surface roughness. In the cutting process diamonds used as a cutting tool in precision machining are of two types' natural diamonds and synthetic diamonds. Natural Diamonds possess slightly better properties over synthetic diamonds but have significant differences in their physical, mechanical and chemical properties. These differences occur due to impurities and internal defects present in the diamond. Synthetic single crystal diamonds are grown in a laboratory from a small diamond seed. Most synthetic diamonds are yellow in color due to higher nitrogen content and trace amounts of left-over metal catalysts from manufacturing.

Single crystal diamond has anisotropic properties owing to the discrete spatial arrangement of atoms. This anisotropic crystallographic orientation causes different mechanical properties in different directions within a single crystal diamond. For diamond tools, the (111), (110), and (100) crystallographic planes are the most commonly used due to their desired optimal characteristic like lower wear rate, lower friction and hardness/softness nature against abrasion wear.

In diamond turn machining, the friction between the tool and workpiece generally relies on the work piece material, temperature and deformation generated at the work piece and tool interface. It was summarized that the friction coefficient μ of diamond is anisotropic and extremely low, in the range of 0.05 to 0.15 [2].

2.3 Diamond tool wear mechanism

Diamond Tool Wear (DTW) is influenced by a wide variety of factors, such as cutting conditions, diamond tool performances, work piece materials, cutting fluids, and gaseous environment. The chemical wear mechanism is the dominant tool wear mechanism during ferrous material cutting and the work piece material is the deterministic factor in the tool wear rate. The chemical wear is mainly governed by high temperatures produced at the interface between diamond tool and work piece, pressures on the diamond surface, catalytic action of work piece, gaseous environment, cooling/lubricating, and activity of the clean surface. Diamond is stable and inert at ambient conditions to most of the metals with/without unpaid d- electrons. During cutting process as the temperature rises, thermal erosion of diamond starts carbon solubility, graphitization, oxidization in oxygen, and chemical reaction with other elements such as Fe Ti, and Si. DTW may appear in any one or combined tool wear forms of flank wear, crater wear, notch wear, nose wear, chipping, groove and fracture.

2.3.1 Graphitization wear

In cutting steel or iron, carbon atoms in the diamond tool graphitizes and this thin graphite film may be scrapped off by the hard particles in the work piece, which causes excessive tool wear during cutting of ferrous metals. Diamond and graphite are the two allotropes of carbon. Diamond is metastable. Graphitization occurs when carbon atoms in the diamond lattice revert to the stable graphite form. The un-catalyzed, graphitization process is exceedingly slow, because atoms must be pulled out from their tightly interlocked sp^3 hybrid orbitals.

Diamond, consists of tetrahedral crystal structure and for graphite, the crystal structure is hexagonal. Under the suitable temperature and pressure conditions, diamond get transformed into graphite as the graphitic from is more stable under these cutting conditions [3, 4]. It was observed that the DTW rate is very high by diamond graphitization while machining of steel [5]. The newly generated clean surface from the machining of work piece activates the graphitization at much lower temperatures. They also observed that the tool wear rate is independent of atmospheric pressure. The researcher introduced that the diamond graphitization may occur at relatively low temperatures (650– 750 °C) due to desorption of chemisorbed hydrogen [6]. It was observed that there is the minimum shear stress required to initiate the diamond graphitization [7]. This value of stress observed was near about of 80–100 GPa. A molecular dynamics model of nanometric cutting pure iron with single crystal diamond tool was made to indicate the essential process of graphitization wear [8]. The results of simulation analysis and experimental detection on diamond worn surface showed the catalytic effect of iron atoms on crystal structure transformation from diamond to graphite. The author reported that the energy barriers for diamond to graphite conversion under normal conditions are very high and the process is forbidden in the normal operating conditions [10]. Although, the graphitization may be initiated in the presence of the metal catalyst under normal operating conditions by providing a lower activation energy path for the forward reaction. He also noted that diffusion follows Fick's law and graphitization follows the Arrhenius law. The model has been successfully applied to predicting conventional tool wear.

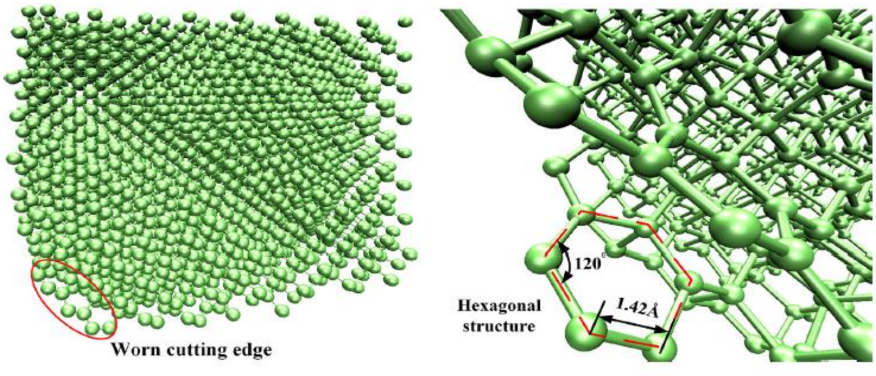

(a) (b)

Fig. 2.1 MD simulation showing (a) worn cutting edge and (b) carbon atoms undergo graphitization at tool tip due to high temperature and pressure [9]

2.3.2 Diffusion wear

The diffusion wear in the diamond tool is caused by high temperature and high pressure and the diffused carbon atom can form interstitial or substitutional solid solutions of carbon in work piece material. Carbon solute atom generally occupy on the interstitial site of iron solvent atom due to the diameter of carbon atom is far less than the diameter of iron atom. The interstitial diffusion process of carbon atoms penetrating into iron lattice is illustrated in Fig. 2.2.

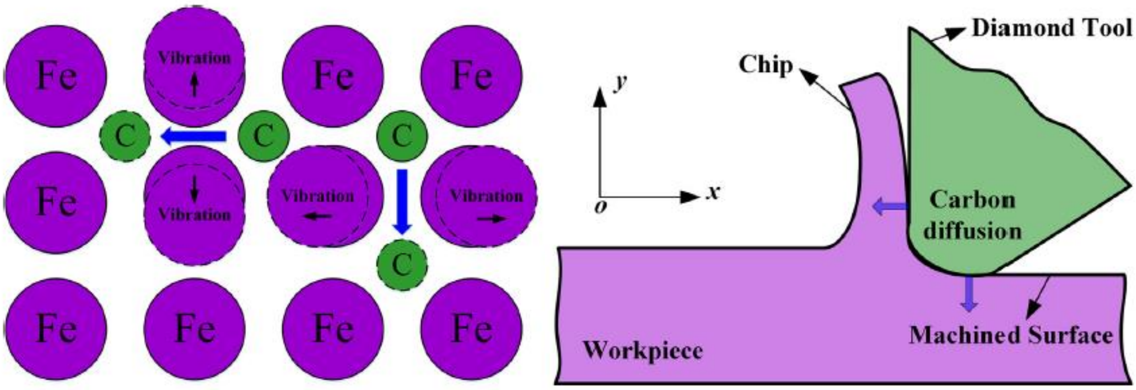

(a) (b)

Fig. 2.2 (a) Carbon atoms diffusion in iron lattice (b) The directions of diffusion form tool tip to workpiece [9]

Researchers found that the cutting temperature affects the diffusion in cutting ferrous metals [11]. The fact that the diffusion increases with rising temperature along with experimental results suggests that diamond diffusion in machining ferrous metals is a crucial factor leading to DTW. the tool wear was predicted with a quantitative equation based on Fick's law, showing that diffusion tool wear obeys' Fick's law of diffusion where the temperatures are under the assumption of 560 °C for Fe and 600 °C for Ni [12].

2.3.3 Oxidation wear

In the ultra-precision cutting ferrous metals with diamond tool, carbon monoxide and carbon dioxide are generated at cutting interface by chemical reactions, which is attributed to the severe plastic deformation and high temperature. Some metallic oxides are also produced on machined surface at elevated temperature due to have a variety of oxidation process caused by two unsaturated electronic configurations of iron atom. These iron oxides get deoxidized by the strong reducing agent under certain conditions and a series of oxidation-reduction reactions occurs at cutting interface which eventually results in oxidation wear of the diamond tool [13].

2.3.4 Fatigue wear

Fatigue tool failure is a mechanical type tool wear and it may occur with any tool and work piece material combination in the appropriate machining conditions. Fatigue failure may lead to chipping and cracking of the tool tip.

2.3.5 Adhesion wear

Adhesion wear occurs by intermolecular attraction forces when diamond atoms comes in contact with workpiece surface and slides on the surface of workpiece. Adhesive wear mechanism proceeds at low cutting temperatures. Adhesion wear is totally different from abrasion wear as it looks as though some diamond materials are torn off from the tool surface, whose surface patterns are concavo-convex and rough.

2.4 Diamond tool wear effects

The single-crystal diamond tool has been employed for UPM due to its excellent performances. A worn diamond tool is still a rigid body that imprints its geometry on the machined surface to influence surface roughness and form accuracy and causes the loss of the original profile accuracy. Micro/nanometric wear can make a significant impact on surface roughness.

A blunt tool will cause cutting forces, especially thrust forces, to increase greatly. The increased cutting forces increase cutting temperature and pressure to promote DTW. Hence DTW and increased cutting forces are mutually promoted by each other. Due to blunt tool edge the cutting mode changes from cutting to ploughing. Ultimately, the loss of the original cutting edge accuracy and the consequent fluctuation in cutting forces will degrade machining accuracy. Increased cutting forces, also promote undesirable vibrations (chatter) and ductile–brittle transition, in the cutting process, which further worsens surface quality and shortens tool life.

2.5 Diamond tool wear controlling

Various diamond tool wear controlling methods with related literatures are described below:

2.5.1 Modulation assisted machining

DTW can be reduced by several orders of magnitude and mirror-quality surface can be obtained by using elliptical vibration cutting [14]. In the study [15,16] researchers developed a 1D ultrasonic vibration-assisted system for Ultra Precision Diamond Turning (UPDT) of hardened steel, which extends tool life significantly with 4-μm flank wear after a cutting distance of 1600 m. They also carried out 2D ultrasonic vibration cutting during UPDT of steel and found that (i) in normal cutting, tool life is very short; (ii) in 2D ultrasonic vibration, cutting forces and surface roughness increase slowly, indicating a low DTW rate, compared with 1D ultrasonic vibration cutting; and (iii) the critical cutting distance in 2D ultrasonic vibration cutting is up to 2000 m, whereas in 1D ultrasonic cutting, it is only about 1000 m. It is stated that ultrasonic vibration cutting yields a reduction of DTW of about two orders of magnitude and diamond tool wear reduction shows the nonlinear relationship with the reduction of effective cutting time/contact time[17]. Researchers [18, 19] found that tool wear in elliptical vibration cutting was less than in ordinary cutting. In his further findings he concluded that in ultrasonic vibration cutting of tungsten-based alloy, increasing the vibration frequency reduces the diamond tool wear. The effect of increasing the vibration amplitude was also similar and it also reduces tool wear. The author reported that the thrust cutting forces generated in the elliptical vibration cutting are much lesser as compared to the conventional ultrasonic vibration cutting and ordinary cutting due to the separating characteristic and the reverse characteristic of the frictional force direction between the rake face of the tool and the chip [20]. The author investigated the effects of the tool nose radius on ultrasonic elliptical vibration cutting in terms of cutting forces, tool wear and surface finish [21]. The experiments showed that 0.6 mm nose radius performs remarkably better when compared to lower and higher nose radius. It was found that low vibration amplitude (<4 μm) and low cutting speeds (<20 m/min) are usually preferred to achieve mirror surface finish [22]. The kinematics of uniaxial ultrasonic-assisted diamond turning hardened steel was studied and pointed out that by increasing the frequency from 40 to 60 kHz, high-quality surfaces and stable cutting process can be obtained [23]. Later, they [24, 25]increased the frequency to 80 kHz and obtained optical surface roughness Ra< 10 nm and a shape accuracy below 300 nm with no clear tool wear.

Researchers developed a 2D finite element model, they found that the cutting forces are directly and significantly affected by the vibration amplitude and the cutting speed, while the resultant temperatures are mostly affected by the cutting speed and not significantly affected by the vibration amplitude [27]. The authors used fly-cutting or milling to control the contact time between the diamond tool and the steel in one cutting cycle by changing the cutting speed and cutting length in each cutting cycle and found that the wear of diamond tool was highly dependent on the tool–workpiece contact time regardless of the cutting speed and can be significantly reduced by decreasing the contact time to less than 0.3 ms [28].

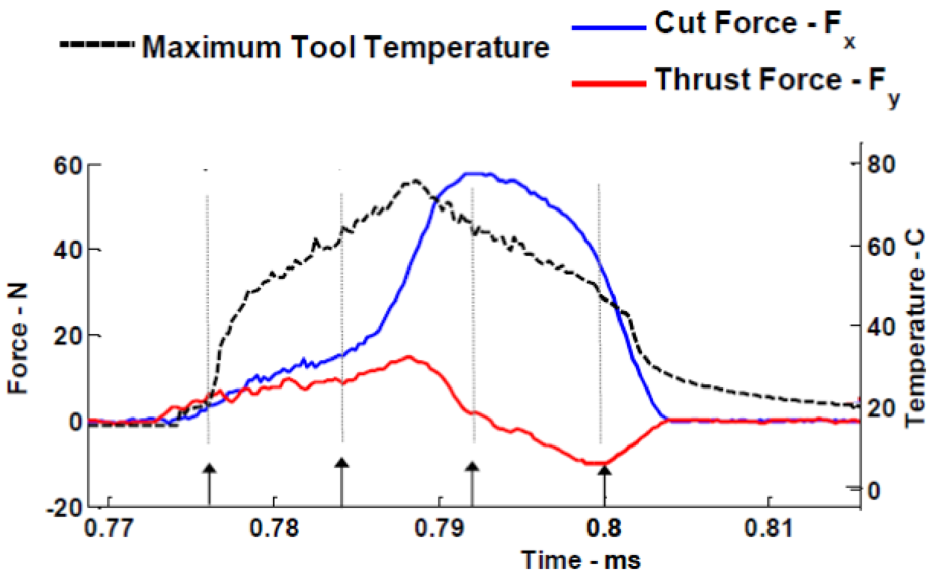

Fig. 2.3 The variation of maximum tool tip temperature, cutting and thrust forces during a cycle of modulation assisted machining (modulation frequency: 10 kHz) of AISI 1118 Steel [26]

A precision vibration-assisted micro engraving system was developed by the integration of Fast Tool Servo (FTS) and ultrasonic elliptical vibration system, which can obtain a good quality of micro-V grooves and reduce cutting force by about 60 % compared with traditional removal process without ultrasonic vibration [29].

2.5.2 Cooling and lubrication of the tool

Cooling plays an important role in decreasing cutting temperatures and surface roughness and prolonging tool life. Since the chemical reaction rate causing tool wear increases exponentially with temperature. Hence, chemical DTW may be retarded significantly in cryogenic machining. The liquid nitrogen was used in machining steel and found that DTW can be reduced by at least one order of magnitude [30]. However, it was impractical since it is difficult to produce high-precision parts due to severe temperature gradients [31].

2.5.3 Protective coatings on the workpiece

Diamond tool coating is also one means of improving tool performances by preventing the direct contact between diamond tool and work piece to extend diamond tool life. The researchers proposed a protective barrier made of perfluoropolyether polymer to protect diamond tools in the machining of titanium [32]. However, the edge radius of diamond tools will become larger after coating, which is not suitable for high-precision components

2.5.4 Gaseous environment for cutting

The cutting steel in carbon-saturated atmosphere and argon atmosphere results in decreased DTW compared to air, because the gaseous oxygen is prevented from reaching the cutting surface and catalyzing wear reaction [33, 34]. The results were in good agreement with the finding which shows that reduced oxygen effectively suppresses the diamond tool wear.

2.5.5 Work piece surface modification

Workpiece modification involves changing the physical and/or chemical behaviors of the machined workpiece. Since it brings down the original properties of the work piece material but it can only be used where work piece material properties alteration can be tolerated. Researchers applied surface modification on the steel and noted that nitrided steel can be diamond turned without excessive DTW [35]. The plasma nitriding treatment was conducted in cutting die steel, which in result reduced the DTW by several orders of magnitude and also produced mirror-quality surfaces finish [36].

2.6 Tool wear models

2.6.1 Tailor model

In conventional cutting, Taylor's equation and its modified/ extended equation have been successfully used to predict tool wear/tool life [37. . In the Taylor equation, the coefficients can be calculated and obtained based on a series of experiments. This empirical method is simple and easy to perform and predicts tool wear before machining. Taylor's basic equation:

$$VT^{n} = C \tag{2.1}$$

C and n are experimentally determined and currently available from many reference sources. T is the tool life; V is cutting velocity. Taylor's extended equation:

$$T = C_2/(V^{p} f^{q} d^{r}) \tag{2.2}$$

All constants (C_2, p, q and r) are experimentally determined. T is the tool life, V is cutting velocity, f is cutting feed and d is depth of cut.

2.6.2 Archard model/Abrasive wear model

Archard derived tool wear law representing contact and rubbing of flat surfaces which shows the abrasive wear of the tool [38.The worn volume (V) described by the Archard Wear Law for abrasive wear depends on sliding distance (d_s), which is the same as the cutting distance. Since the wear on a diamond tool occurs primarily on the flank face, the average flank force (F_f) is used as the acting normal force in the Archard wear formulation.

$$V = A_w . w = k . F_f . d_s \tag{2.3}$$

A_w is the 2D worn area and w is the tool worn width [39].

2.6.3 Arrhenius Model/Graphitization model

Many researchers have proposed wear models that relate tool wear to temperature in Arrhenius type equation [26. . The tool wear equation can be written either of the interchangeable forms describing wear /time:

$$\frac{dW}{dt} = A \exp\left(\frac{-E_a}{RT}\right) \tag{2.4}$$

Where W is worn volume, E_a is the activation energy, A is the pre-exponential constant, v_s is the sliding speed of a tool against a workpiece, R is the universal gas constant and T is the tool tip temperature.

The above equation can be written in the wear /distance form also as follows:

$$\frac{dW}{ds} = \frac{A}{v_s} \exp\left(\frac{-E_a}{RT}\right) \tag{2.5}$$

2.7 Numerical simulation of cutting

Cutting simulations are widely used to study and predict behavior of various materials under different cutting conditions with combinations of different tool geometries. 2D (orthogonal) and 3D (oblique) simulations are performed using various numerical methods. Finite Element Method (FEM) is the most common method to simulate cutting. The researchers conducted orthogonal cutting experiments and a simulation analysis of ultrasonic elliptical vibration cutting to find out the effect of upward friction force on the chip morphology [41]. Arrhenius wear model was used to predict the diamond tool wear in elliptical cutting process. Experiments were conducted over wide range of cutting speeds on the AISI 1215 steel to evaluate the activation energy for the material lying between 25 kJ/mol and 29.3 kJ/mol. The tool tip temperature generated from the FEA modelling of the process was used as input parameter for tool wear model [42]. A numerical simulation technique was developed to evaluate the tool temperature and normal stress acting on the wear surface. It is demonstrated that tool wear is attributed to the abrasive wear mechanism, but the effect of the adhesion wear mechanism is minor in nano-groove machining [43].

2.7.1 Material constitutive model

One of the most important subjects in metal cutting simulation is modeling flow stress of work piece material properly in order to obtain true results. Flow stress is an instantaneous yield stress and it depends on strain, strain rate and temperature and represented by mathematical forms of constitutive equations.

2.7.2 G.R. Johnson & W.H. Cook

This research describes material behaviors undertaking large strains, high strain rate and temperatures [44]. It calculates the flow stress of work material with the product of strain, strain rate and temperature effects that are individually determined as

Johnson-Cook hardening is a type of isotropic hardening where the static yield stress σ_0 is assumed to be of the form

$$\sigma_o(\epsilon, \dot{\epsilon}, T) = [A + B\epsilon^n][1 + C\ \ln \dot{\epsilon^*}][1 - (T^*)^m] \tag{2.6}$$

Where ϵ is the equivalent plastic strain, which is calculated in dependence of the strain tensor, $\dot{\epsilon}$its time derivative, the plastic strain-rate, and A the material yield stress. B and n are strain hardening parameters, C a strain rate parameter, and m a temperature coefficient.

The normalized strain rate and temperature are defined as:

$$\dot{\epsilon^*} = \frac{\dot{\epsilon}}{\dot{\epsilon_o}} \tag{2.7}$$

$$T^* = \frac{(T - T_o)}{(T_m - T_o)} \tag{2.8}$$

where $\dot{\epsilon_o}$ is a user-defined plastic strain rate, T_o the reference temperature, and T_m the reference melting temperature.

2.7.3 Oxley Material Model

Oxley **[44]** used power law to represent material flow stress for carbon steel as $\sigma = \sigma_1 \varepsilon_n$ where, σ & ε are flow stress and strain σ_1 is material flow stress at $\varepsilon = 1$, n is the strain hardening exponent further σ_1 & n depend on velocity modified temperature ($T_{mod.}$)

$$T_{mod} = T(1 - \vartheta \log(\frac{\dot{\varepsilon}}{\dot{\varepsilon_o}})) \tag{2.9}$$

Where ϑ & $\dot{\varepsilon}_o$ are work piece material constant.

2.7.4 Zerilli and Armstrong Material Model

Two micro- structurally based constitutive equations were developed [44]. They worked on face-centred cubic and body-centred cubic metals to analyse their temperature and high strain rate responds and noticed a significant difference between these materials. Therefore, they developed two distinct models. The constitutive equation for BCC metals can be written as follows

$$\sigma = C_o + \; C_1 e^{(-C_2 T + C_4 T ln(\frac{\dot{\varepsilon}}{\dot{\varepsilon}_o})} + C_5 \varepsilon^n \tag{2.10}$$

Flow stress for FCC metals is defined as

$$\sigma = C_o + \; C_2 \varepsilon^{-1/2} e^{(-C_3 T + C_4 T ln(\frac{\dot{\varepsilon}}{\dot{\varepsilon}_o})} \tag{2.11}$$

In these equations, C_o is component of stress that accounts for dislocation density on the flow stress, $C_1 – C_5$, n are material constants and T is the absolute temperature. In equation 2.5 it is assumed that the strain dependence on flow stress is not affected by strain rate and temperature while it is opposite in equation 2.9.

2.8 Gap areas

Mechanism of MAM on hardened steel is not well researched and published. The effect of MAM parameters on tool wear of SCD while machining hardened steel is not well investigated. Effects of MAM on the surface finish are not well understood. Effects of MAM on residual stresses are not studied and the effect of contact time on the tool wear is not well studied.

Chapter 3
FEA modeling and validation of tool wear for conventional cutting

3.1 Introduction

For this modelling and subsequently simulation of orthogonal metal cutting of hardened steel as work-piece and Single Crystal Diamond (SCD) as cutting tool, a Finite Element Analysis (FEA) was used. The work material is hardened steel and its flow stress is modelled as a function of strain, strain rate, temperature to reflect realistic behaviour. The entire cutting process is discretized into many small-time increments and in every small-time increment, dynamic and thermal analysis procedures based on the implementation of an explicit integration rule were carried out (coupled temperature- displacement analysis). The wear model obtained from literature requires machining parameter viz. temperature at the tool tip as input for calculation of tool wear rate. The tool tip temperature is evaluated with the FEA model for the prediction of the tool wear.

3.2 Formulation of numerical model

Diamond turning is a complex operation and modelling its real behaviour is very difficult i.e. taking into account the entire factor at same time following assumptions are made in this analysis.

i. The motive of first assumption is to simplify 3D machining to 2D orthogonal machining as shown in Fig. 3.1. It is reasonable because the depth of cut (DOC) of the micro scale cutting is very small; deformation zone is very small as compared to tool and work-piece size, sometimes only several microns. Under these conditions oblique angle 3D cutting process has very little effect and can be ignored and depth of cut can be taken as constant. Therefore, depth of cut in 3D is represented by uncut chip thickness in 2D.

ii. Material strengthening effect due to micro-scale cutting has been neglected. Flow stress is taken as independent of scale variable. Only strain, strain rate and temperature effects are taken for material modeling.

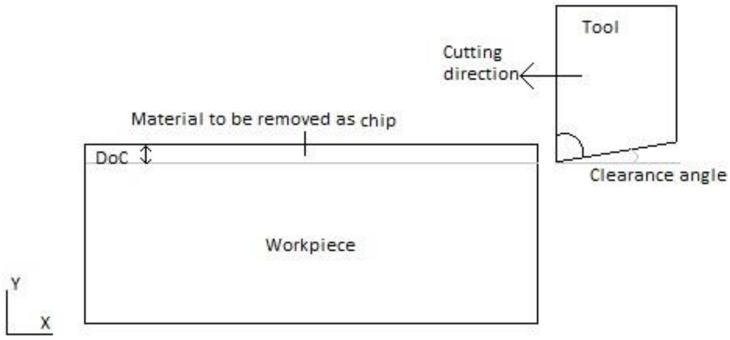

Fig. 3.1 Equivalent 2D model

iii. A Plain strain condition was assumed.

The present work focus on 2D FE modeling of chip formation based on orthogonal cutting, although two-dimensional approach is restrictive approach from practical view point but it reduces computational time and provide satisfactory result regarding chip formation.

The geometric model, meshing and boundary condition are defined later in this chapter. Work-piece is constrained in X & Y direction and tool is given velocity in -X direction. A chip separation criterion is critical issue in simulation process. In this regard chip separation is visualized with ductile damage model. During solving process, when equivalent plastic strain exceeds critical value damage, an initiation criterion is met. Once the element satisfies damage initiation criteria, it is assumed that progressive degradation of material stiffness occurs, leading to material failure based on damage evolution. The flow chart is described in Fig. 3.1

3.3 Material constitutive model

One of the most important subjects in metal cutting simulation is modeling flow stress of work piece material properly in order to obtain true results. Among others, the most widely used one in metal cutting simulations is Johnson-Cook material constitutive model is a particular type of Misses plasticity model with analytical forms of the hardening law and rate dependence and is suitable for high strain rate deformation of many materials, including most

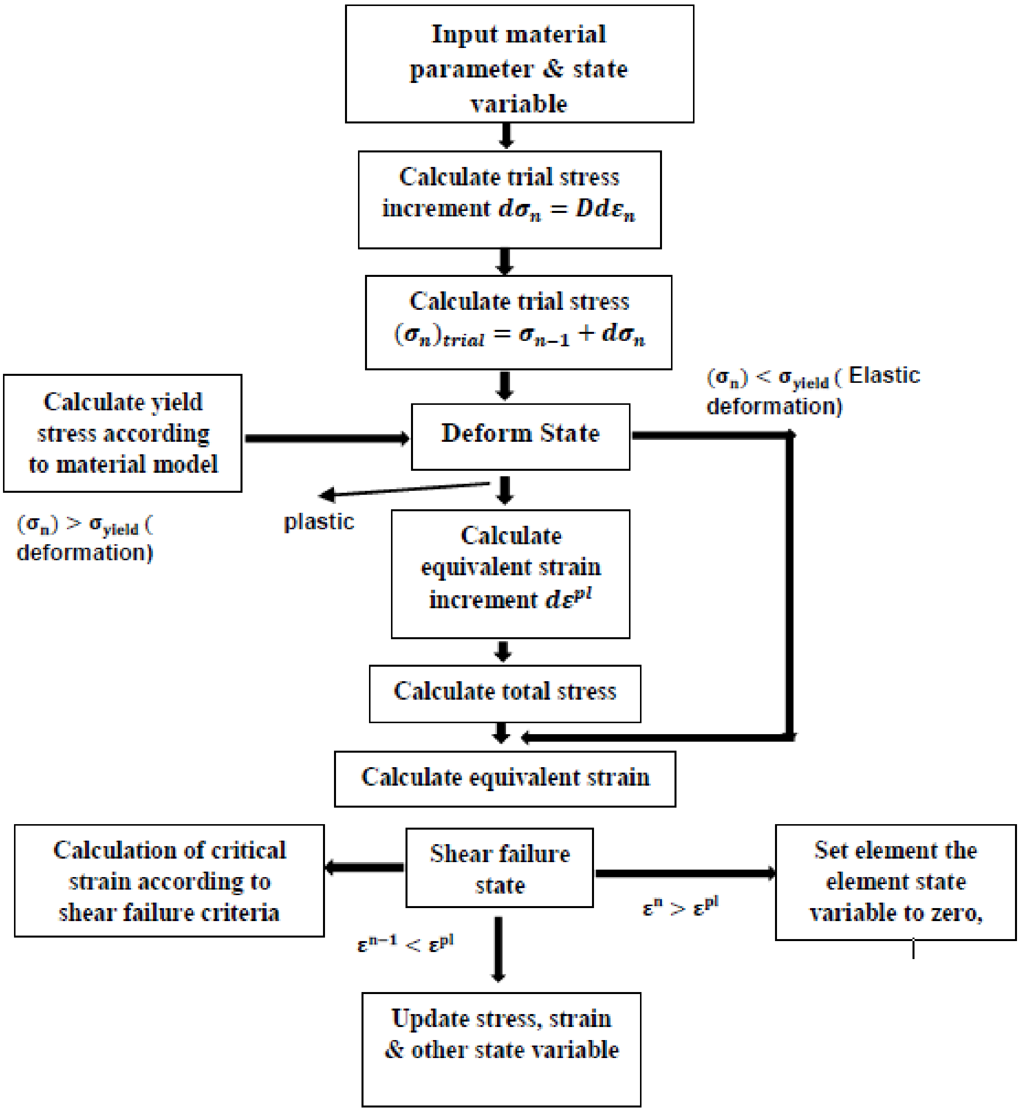

Fig. 3.2 Flow chart for numerical simulation

metals and is typically used in adiabatic transient dynamic simulation and can be used in conjunction with Johnson Cook dynamic failure model. The material used in this study is AISI 1045 and its JC material parameter is shown in the table 3.1.

Table 3.1 J-C parameter for AISI 1045 [46]

A(MPa)	B(MPa)	C	n	m	$\dot{\epsilon}_o[s^{-1}]$	T_m (℃)	T_o (℃)
533	600	0.0134	0.234	1.0	0.001	1460	20

The Johnson-Cook dynamic failure model is based on the value of the equivalent plastic strain at element integration points; failure is assumed to occur when the damage parameter exceeds 1.

Table 3.2 Johnson-Cook Damage coefficients [46]

D_1	D_2	D_3	D_4	D_5	$\dot{\varepsilon}[s^{-1}]$
0.05	4.22	-2.73	0.0018	0.55	1

During machining heat is generated in primary shear deformation zone due to severe plastic deformation and in secondary zone due to both plastic deformation and friction in tool chip interface. Frictional work conversion factor considered as 1.0. The value of the fraction of the thermal energy conducted into the chip may vary within a range, say, 0.35 to 1 in the present work, 0.5 has been taken for all. It is applicable only to adiabatic thermal-stress analysis, fully coupled temperature-displacement analysis.

3.4 Details of modeling and simulation

A 2D orthogonal explicit thermo-mechanical model is being developed in FEA analysis. In present study both cutting tool and work-piece are considered as 2D deformable bodies. The tool has 0° rake angles, 6° clearance angles and 200 nanometer nose radiuses. Tool material was selected as Single Crystal Diamond (SCD), Thermal and mechanical properties of SCD are given in the Table.3.2. Since the temperature rise during micron and submicron diamond cutting is less so the properties can be taken as constant with respect to temperature.

Table 3.3 Tool Material Parameters

Parameter (units)	**Description**	**Value**
E (GPa)	Young’s Modulus	1210
ρ_o (Kg/mm^3)	Density	3.52×1e-6
μ	Poisson’s ratio	0.22
C_p (joule/(Kg-K))	Specific heat	520
K (watt/(m-K))	Thermal conductivity	2000
α[μm/(m°C)]	Thermal expansion	0.7

The mechanical and physical properties of the AISI 1045 steel [46] are shown in the table 3.4.

Table 3.4 AISI 1045 properties

Parameter (units)	**Description**	**Value**
E (GPa)	Young's Modulus	200
ρ(Kg/m^3)	Density	7800
μ	Poisson's ratio	0.3
C_p (joule/(Kg-K))	Specific heat	486
K (watt/(m-K))	Thermal conductivity	49.8
α[µm/(m°C)]	Thermal expansion	11.5
T_m [°C]	Melting temperature	1460

3.5 Meshing of tool and workpiece

Finite element mesh of work piece is modeled using and total number of element is 43264 with 5600 as a 4 nodded linear quadrilateral element of coupled temperature displacement for chip formation. The work piece is created at 1.0 mm long and 0.5 mm high compare to microns of chip size therefore the predicted results are not sensitive to the displacement boundary conditions and steady state can be reached. Mesh of deformation zone is modeled very dense. Finite element mesh of tool is modeled using 253 elements out of which 245 linear quadrilateral elements of coupled temperature displacement and 8 linear triangular elements for the analysis. The distribution of mesh on tool is not uniform. Mesh density of tool tip and a part of rake face are modeled high with using free meshing technique and differential number of seeds is given, to obtain more accurate temperature distribution results as shown in Fig. 3.3 in order to reduce calculation time and obtain more accurate results. As the large deformation and deformation rate in the workpiece are involved in the cutting process, arbitrary Lagrangian–Eulerian (ALE) formulation with the advancing front algorithm is used to provide the mesh distortion control in every analysis increment to avoid excessive mesh distortion.

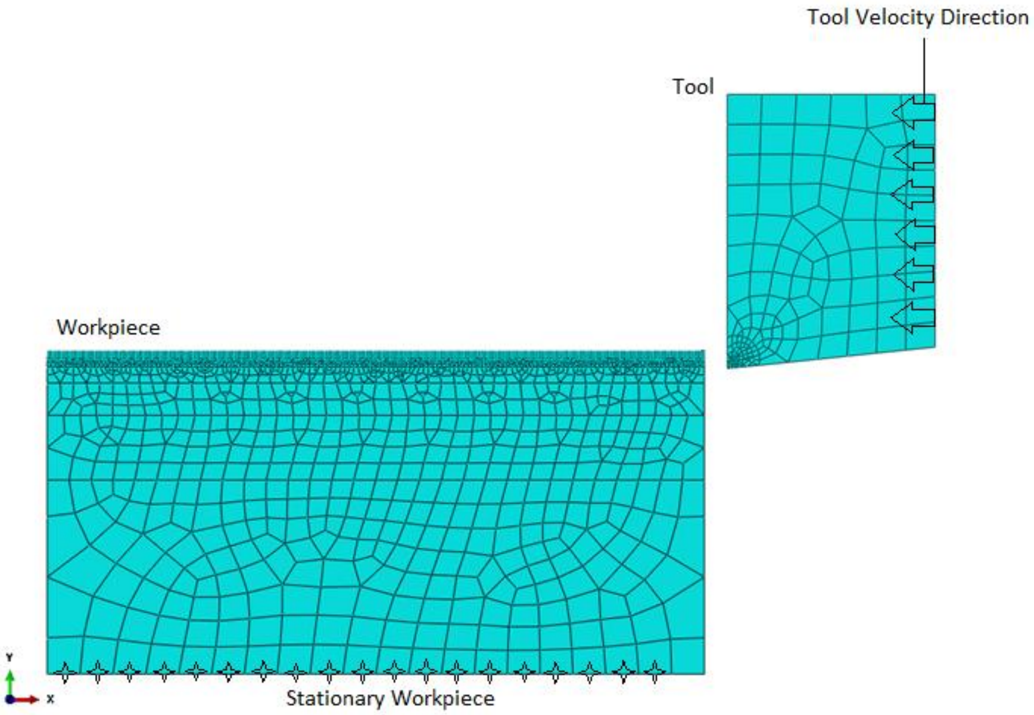

Fig. 3.3 Meshed Workpiece and tool

3.6 Properties of mating surfaces

The interaction between contacting body is defined by assigning a contact property; it defines tangential behavior (friction), conductance and normal behavior. Tangential behavior includes friction model that defines the force resisting the relative tangential motion between surfaces. Normal behavior includes a definition for the contact pressure–over closure relationship that governs the motion of the surfaces. In addition, a contact property inhibits information about thermal conductance, thermal radiation, thermal convection and heat generation due to friction. In this study, a kinematic contact algorithm has been used to enforce contact constraints in master–slave contact pair, where rake surface of the cutting tool is defined as the master surface and chip as the slave (node-based) surface. Both the frictional conditions and the friction-generated heat are included in the kinematic contact algorithm through tangential behavior and gap heat generation modules of the software. Based on commonly used coulomb’s law mean friction coefficient is taken as 0.2. Further convective heat loss to environment is given by defining thermal film coefficient as 10 and ambient temperature is taken as 293K.

In this study coupled- temperature displacement explicit dynamic analysis is used. A thermo mechanical analysis is a nonlinear calculation in which the displacements and temperatures are simultaneously solved. In this way the reciprocal action of the temperature on the displacements and the displacements on the temperature can be taken into account. In this module associated output request can also be created. An output request contains information regarding which variable will be obtained as output.

3.7 Results

During cutting, work-piece material undergoes severe plastic deformation in primary shear zone which acts as the main source of heat generation in the tool along with friction. The material in the chip underside deforms plastically under the pressure and friction of the cutting tool face. Higher plastic strain causes higher temperature generation in the primary shear zone as compared to the other part of the chip. This heat along with the heat generated due to friction between tool rake face and chip, gets transferred to the tool tip and rises its temperature. Under steady state condition the heat coming and going out of the tool becomes almost stable and provide a steady state temperature to the tool tip. This steady state temperature at the tool tip depends upon the process parameters like cutting velocity, depth of cut, feed rate, coolant etc. Here in the simulation temperature profile variation are caused by the two main parameters defining tool tip temperature namely cutting velocity and depth of cut of the process. The Fig. 3.4 shows temperature profile generated during conventional cutting with 1 micron depth of cut.

3.7.1 Tool tip temperature profile for different depth of cut and cutting velocities

Temperature at tool tip varies with depth of cut and cutting velocity of the process. The Fig. 3.5 shows the variation in the steady state temperature generated for some cutting velocity and depth of cut combinations. The fluctuations in the temperature during steady state are caused by the finite size of the mesh of the work piece. Since the work piece elements have some finite size and the heat is generated when each element is sheared during metal cutting process, some amount of heat is added to the tool during each step of simulation which rises its temperature. On the other hand, some amount of heat is transferred to the atmosphere due to applied boundary conditions which reduces the tool tip temperature. Under steady state this ups and down in the heat flux causes temperature rise in the periodic manner.

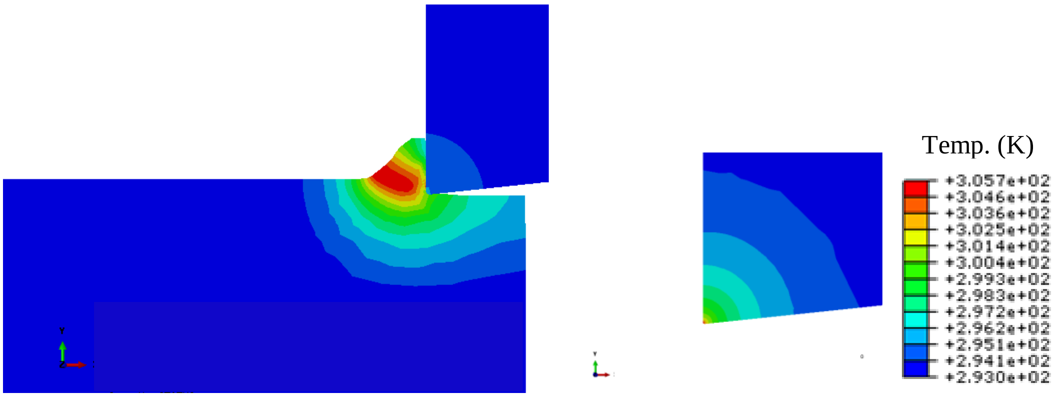

Fig. 3.4 Temperature contours for AISI 1045 steel cutting with SCD for 1 μm depth of cut, 1 m/s simulation results (a) for whole model (b) for tool tip.

But as the mesh elements becomes non uniform in size after deformation in the shear zone some random factor of the temperature is added to the periodic fluctuation in the tool tip temperature. The overall tool temperature profile fluctuations of the tool are caused by these two factors and should become almost negligible when mesh size is reduced to approx. zero value. Generally mesh elements size is limited by the computation time and acceptable vales of temperature generated during cutting process. The temperature generated at tool tip in diamond cutting process are relatively smaller as compared to ceramic and other tools due to very high value of thermal conductivity/ diffusivity of the diamond. Diamond has thermal conductivity (2000 W/m/K) of approx. forty five times higher than the steel (49W/m/K).

3.7.2 Comparison of tool tip temperature variation for varying DOC's and cutting velocities

Eight numbers of simulations are done to show the value of the tool tip temperature generated for 1 and 2 microns depth of cut and 0.5, 1, 2 & 3 m/s cutting velocities. The value of the tool

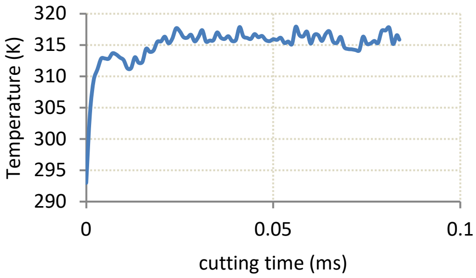

(a) 1micron-2m/s

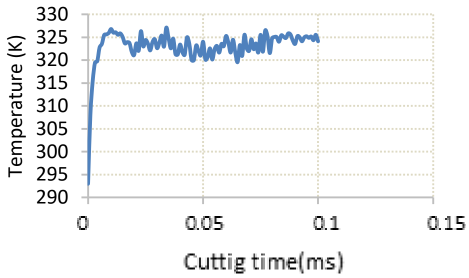

(b) 1.5microns-2m/s

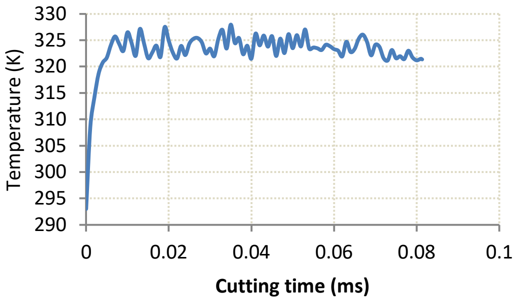

(c) 2 microns-2m/s

Fig. 3.5 Steady state temperature during various cutting conditions for 1, 1.5 and 2 microns depth of cut and 2 m/s cutting velocity (a) 1micron-2m/s, (b) 1.5microns-2m/s and (c) 2 microns-2m/s

tip temperature taken from literature is the FEA simulation values which are used to predict the tool wear with the help of Arrhenius tool wear equation. Arrhenius tool wear equation takes the tool tip temperature values as one of the input parameter for the wear prediction The tool tip temperature variation with respect to different velocities is shown in the Fig. 3.6(a), (b) and (c).

The Fig. 3.7 shows the rise in the tool tip temperature for diamond tool and CBN tool for similar cutting conditions during conventional cutting. Two points observed are mentioned below:

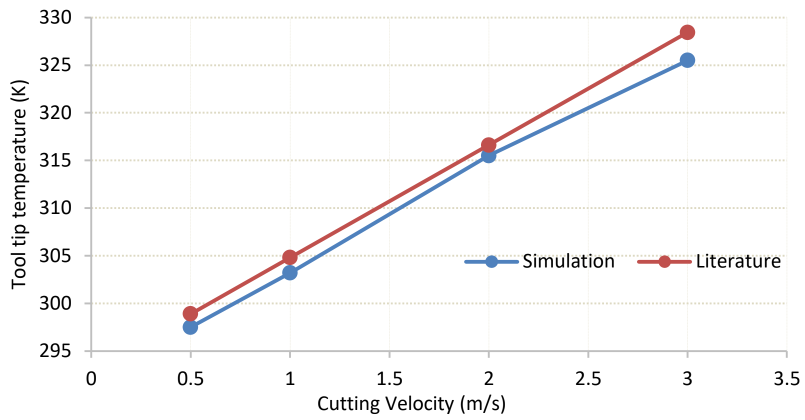

(a) FEA simulation comparison 1 micron DOC

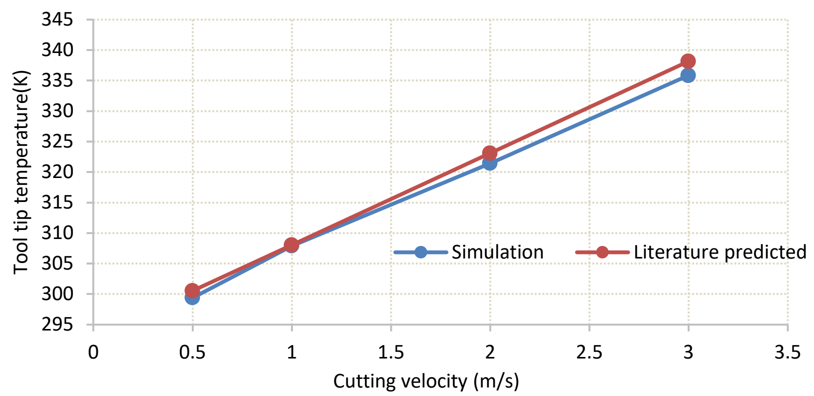

(b) FEA comparison for 1.5 microns DOC

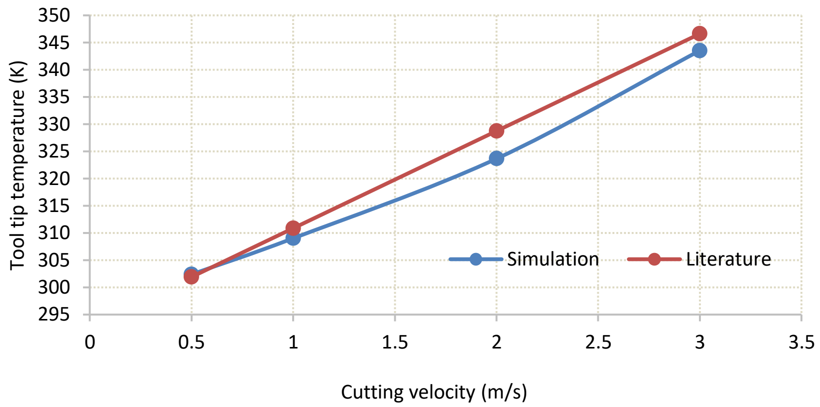

(c) FEA Comparision for 2 microns DOC

Fig. 3.6 Tool tip temperature variation with tool cutting velocity (a) 1 micron,(b) 1.5 micron and (c) 2 micron depth of cut

i. Temperature rise in CBN tool is much higher (ΔT=157 K) as compared to diamond tool (ΔT=31 K), this is due to high thermal diffusivity/ conductivity value of diamond compared to CBN. Diamond has thermal conductivity of 2000 W/m/K compared to CBN which has this value of 20 W/m/K.

ii. The fluctuations in the tool tip temperature are much lesser in the CBN tool due to its low value of thermal diffusivity (6.37e-6m^2/s) as compared to diamond tool (1.09e-3m^2/s). Thermal diffusivity defines the rate of transfer of heat of a material from the hot end to cold end.

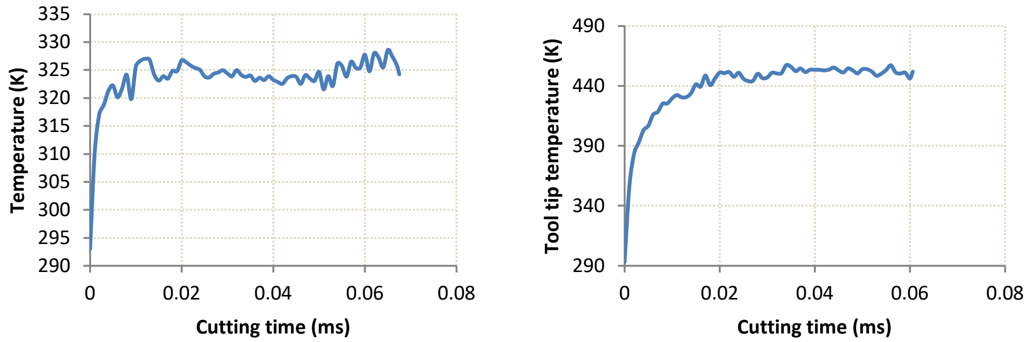

(a) Diamond tool: 1 micron- 3m/s (b) Ceramic tool: 1micron-3m/s

Fig. 3.7 Tool tip temperature rise during conventional cutting of AISI 1045 steel (a) Diamond tool and (b) Ceramic tool

3.8 Literature validations of tool wear for conventional cutting

To generate Arrhenius tool wear equation author [26] conducted multiple experiments, at work piece velocities ranging from 0.001 – 4 m/s. All work pieces were AISI 1215 steel machined from the same stock. In the low speed experiments (2-8 mm/s), work piece velocity was set directly by the DTM axes. Diamond tool wear was measured in an SEM using the Electron Beam Induced Deposition (EBID) method.

Wear rates between zero cut distance and the first cut distance created a first rate value or slope. Rates between the first and second cut distance create a second slope. The two slope values calculated are shown in the Table 3.3. So for the literature validation of the simulated results, two values of Arrhenius wear constants can be proposed. The preferred value for a particular validation can be chosen based upon cutting distance travelled by the tool. First slope values were taken at starting of the experimental results (under 25m cutting distance) and thus predict the better results while the cutting distance is less than 25m. The second slope can be used for the higher cutting distances. Using the two different values of Arrhenius constants predicts better results than taking a mean or using same slope for all cutting speeds.

Table 3.5 Arrhenius' wear constants

	E_a (kJ/mol)	A (μm^2/sec)
First slope	24.95	311.1
Second slope	29.31	330.3

Since high and medium work piece speed experimental data were used in equation prediction those values cannot be used for its cross validation. Instead of that here tool wear data for low cutting speed is used which was not used in the equation prediction since the variation is the temperature was very low. The low rise in the tool tip temperature, those points would lie at the same x-axis location on an Arrhenius plot and not provide for determining the Arrhenius coefficients. Although the same data could be used to cross validate the model with experimental results.

From the available experimental data 4mm/sec and 8mm/sec cutting speed experimental tool wear values were taken to cross validate the model. The values of the tool wear can be calculated by multiplying the wear rate per unit distance ($\frac{dW}{ds}$) with cutting distance. The above mentioned method is valid when the tool wear varies linearly with time/cutting distance.

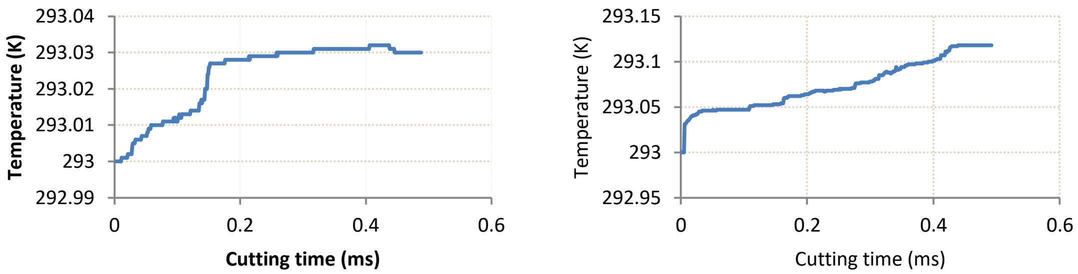

(a) 4 mm/s (b) 8 mm/s

Fig. 3.8 Simulated value of tool tip temperature with (a) 4 mm/s and (b) 8 mm/s cutting velocities, AISI 1045 steel and SCD diamond tool

The tool tip temperature variation for the wear calculation form the FEA model conducted are shown in the Fig. 3.8 The temperature rise at these cutting values are low, this is due to very high thermal diffusivity of the diamond tool.

3.9 Tool wear prediction

The comparison of the tool wear rate and tool wear values predicted by FEA simulation and Literature values of tool wear is shown in the Fig. 3.9 and 3.10 Since the cutting distance taken for validation is under 25m distance the first slope value is chosen for the comparison shown in the table 3.5.The bar charts contain simulated values from FEA model and literature values from experiments. Wear rate values are shown in green color and wear values in orange color. Wear values can be calculated by multiplying the wear rate with cutting distance. In the literature 5 m of cutting distance was taken after starting point for wear measurement, so corresponding values are shown in the Fig. 3.9 and 3.10 for cutting speed of 8 mm/s and 4 mm/s respectively. The wear rate and wear values from the simulation can be compared with the corresponding literature values in each Fig.. The simulated results wear rate/wear (for 8 mm/s and 4 mm/s) shows variation within 30% form the literature values of wear rate/ wear values.

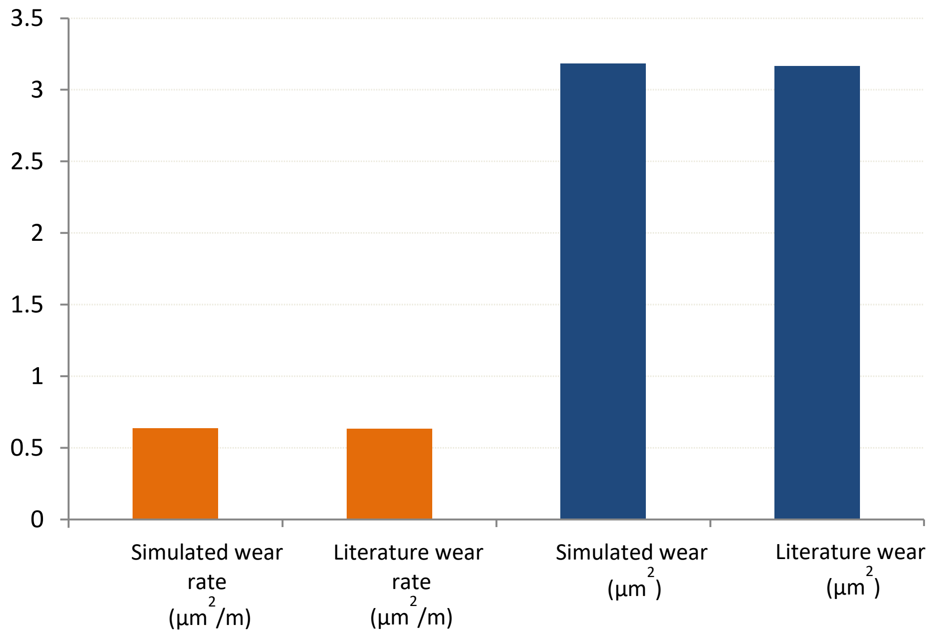

Fig. 3.9 Tool wear rate and tool wear values for 8 mm/sec and 1 micron depth of cut values after 5m of cutting distance

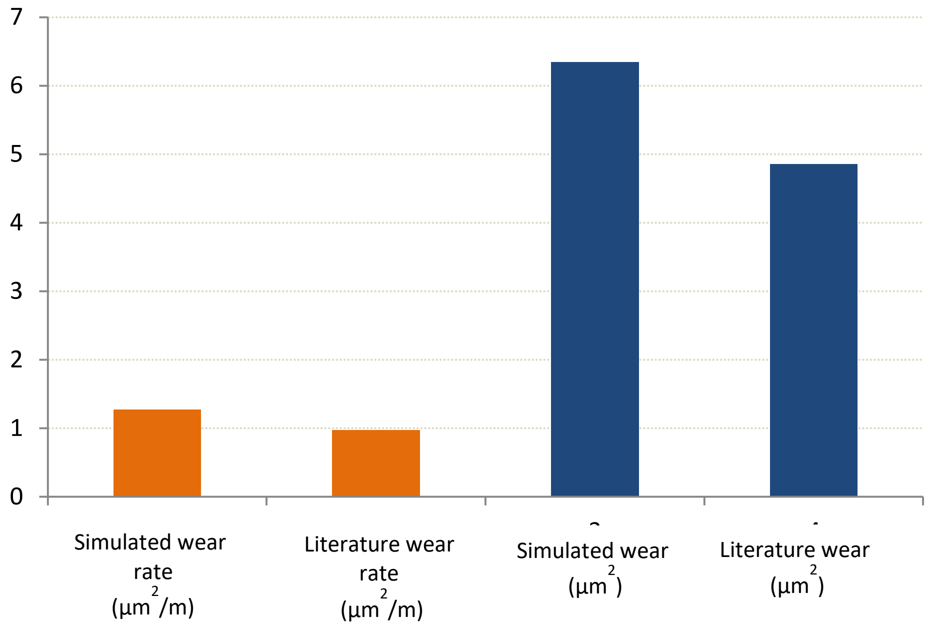

Fig. 3.10 Tool wear rate and tool wear values for 4 mm/sec and 1 micron depth of cut values after 5m of cutting distance

3.10 Cutting forces prediction

The Cutting forces evaluated from FEA simulation were compared with the Literature cutting forces. Fig. 3.11 shows the cutting/principal force and thrust forces generated on the tool for linear cutting process with DOC 1 micron and cutting velocity 2.31m/s for the 1045 Steel[48]. The literature values of cutting and thrust force were recorded for 1215 steel (Fig. B.1 from Appendix B) under same conditions; here both steel grades are taken as equivalent to each other. Although during experiment the value of these forces increases with cutting distance due to the tool wear. In both Fig. 3.11 and B.1 from Appendix B the X axis is different; one shows time and another cutting distance. Still the values of forces can be compared since these do not change for particular cutting conditions and depends upon chip shape and workpiece properties. Although in actual experiment for high cutting distances force values may increase slightly as the tool tip wear out.

The Bar charts shown in the Fig. 3.9 and 3.10 shows that the FEA model demonstrated for the validation of tool wear predicts acceptable results (<30 % deviation) and further can be used for the Elliptical cutting model for tool wear prediction. This deviation in the simulated and literature value may occur due to various assumptions that FEA model of tool wear has used.

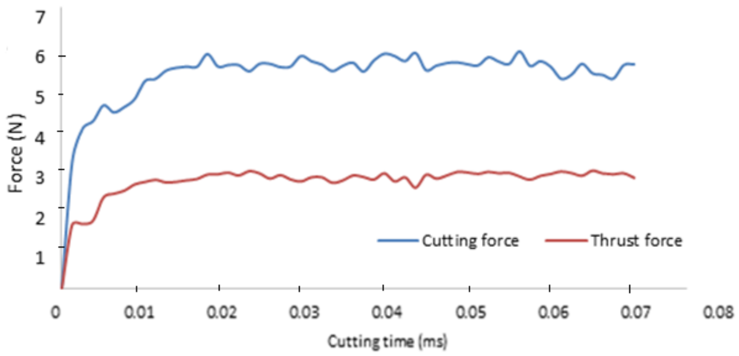

Fig. 3.11 Forces Simulated while cutting 1045 steel

The Fig. 3.11 and B.1 show the variation of cutting forces generated during cutting process. Although the values in the literature values increases with time due to tool wear increases the cutting forces. In the FEA values since the tool maintains its sharpness the cutting forces remains constant through a particular simulation after full chip is formed.

Chapter 4
Numerical modeling and validation of tool wear in elliptical cutting

4.1 Introduction

It was discussed in the literature survey that diamond tool undergoes chemical wear while cutting the ferrous materials, the same phenomena was proved with FEA model in chapter 3 for conventional cutting process. Literature proposed many methods to reduce the diamond tool wear for cutting of ferrous materials. Modulated Machining is one of the most suitable methods for reducing the tool wear without compromising the surface finish of the work piece. The FEA modeling and simulation validation with literature data of the Modulated machining for the cutting of ferrous material (steel) was performed. As the modulated machining contains many controlling parameters apart from feed, depth of cut and cutting velocity, the process becomes complex in nature. The impact of various cutting parameters like cutting frequency, modulation amplitude, High speed ratio, contact time etc. also needs to be studied on the tool wear. The Cross validating of the FEA model of tool wear in case of elliptical cutting with literature results was conducted.

4.2 FEA model of elliptical cutting

For elliptical motion, tool was given displacement condition with desired cutting frequency and amplitude in X and Y both directions to generate desired elliptical tool path. Workpiece was given velocity condition to simulate the cutting velocity given in the actual experiment. To give an overall idea of the elliptical cutting process and variation in the tool tip temperature and cutting forces, elliptical cutting process for DOC: 2 micron, frequency: 10 KHz, ellipse amplitude: 11×2 micron (half major axis× half minor axis), $v_{wkpc} = 0.1 m/s$ is shown. Here in the Fig. 4.1 (a) to (d) shows various steps with tool tip temperature in cutting process.

a) The tool comes into contact with workpiece the temperature raises in the primary shear zone due to high strain.

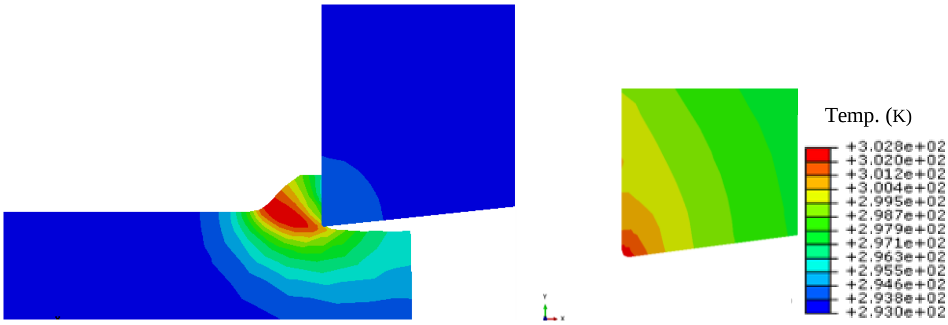

(a)

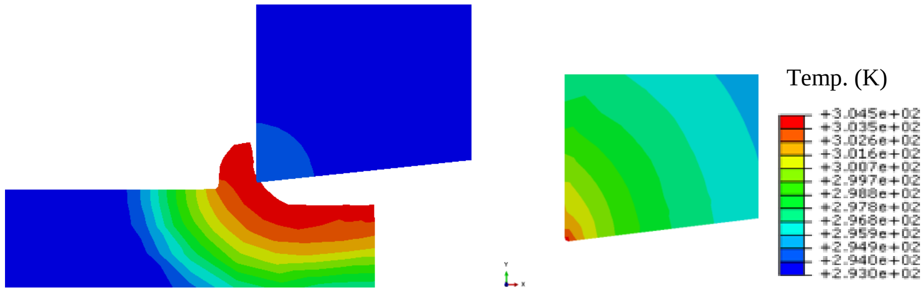

(b)

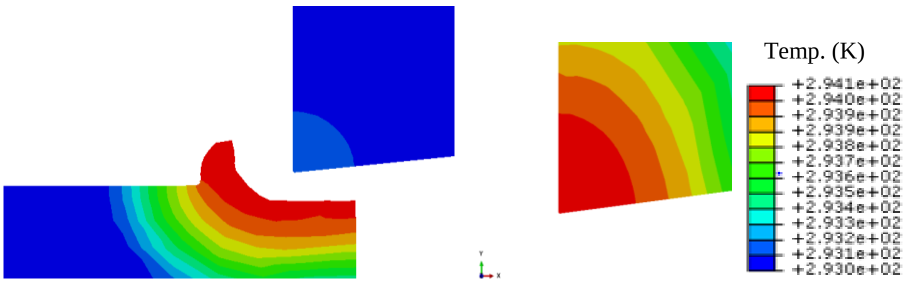

(c)

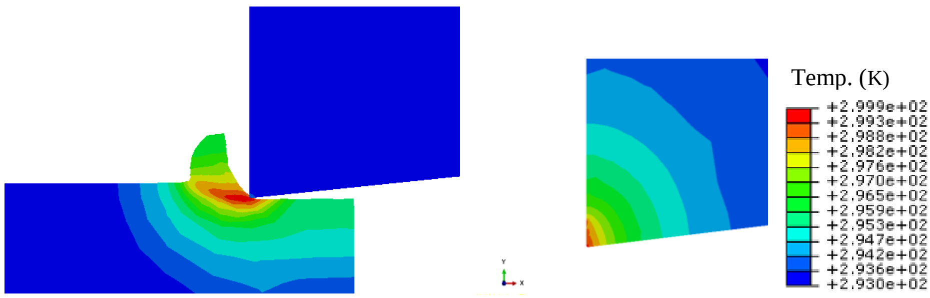

(d)

Fig. 4.1 Steps of Elliptical cutting of AISI 1045 with SCD tool, cutting parameters: DOC: 2 micron, frequency: 10 KHz, ellipse amplitude: 11×2 micron from (a) to (d)

b) The tool following the elliptical path and cutting the workpiece, the temperature of the workpiece and tool increases due transferred heat to tool.
c) The tool got separated from the workpiece and tool temperature drops due to convection to surroundings.
d) The tool starts new cycle and cycle back to step (a) and the process continues.

4.3 Cutting and thrust force variation

The variation of the cutting and thrust force produced during cutting is shown in the Fig. 4.2. Since the uncut chip geometry and material strength remains same for the whole process the cutting forces produced also repeats there pattern. The maximum values of the cutting and thrust forces do not change with time for a particular process. The thrust force in the process takes negative values. That means the tool tries to push up the workpiece and the thrust force value changes to opposite direction.

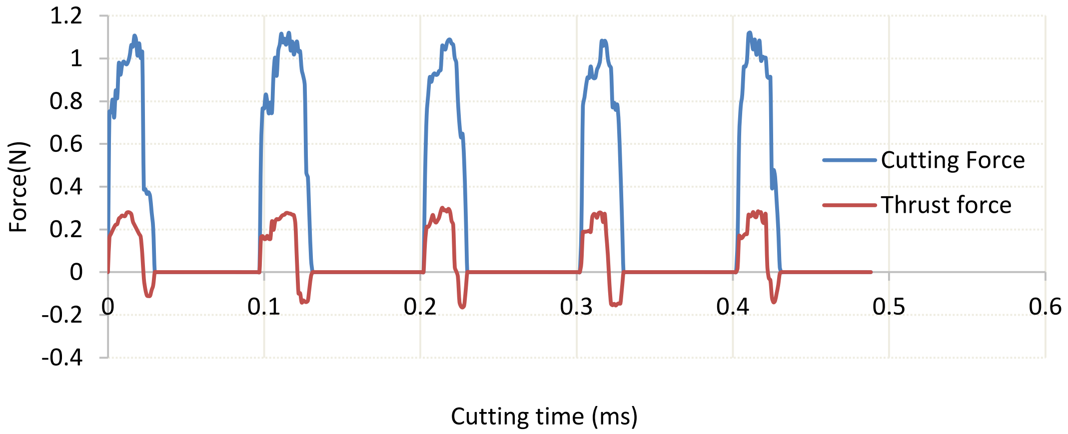

Fig. 4.2 Variation in the Cutting and thrust forces during elliptical cutting, material AISI 1045 with SCD tool, cutting parameters: DOC: 2 micron, frequency: 10 KHz, ellipse amplitude: 11×2 micron

The direction reversal of the thrust force during elliptical cutting is caused by the change in the direction of kinetic friction force between chip and the tool's rake face. When the velocity of the tool in the Y direction becomes more than the chip velocity in Y direction, the friction reversal takes place. (As shown in the Fig. 4.3) This friction force tries to resist the tool motion in +Y direction which cause the thrust force reversal. This phenomenon happens due to the reversal of the direction of the chip velocity with respect to the rake face of tool. The same phenomena is reported in the previous work of elliptical cutting simulations proposed by B M lane [26] and Shamato[45]. This phenomenon is further explained using following mathematical expression.

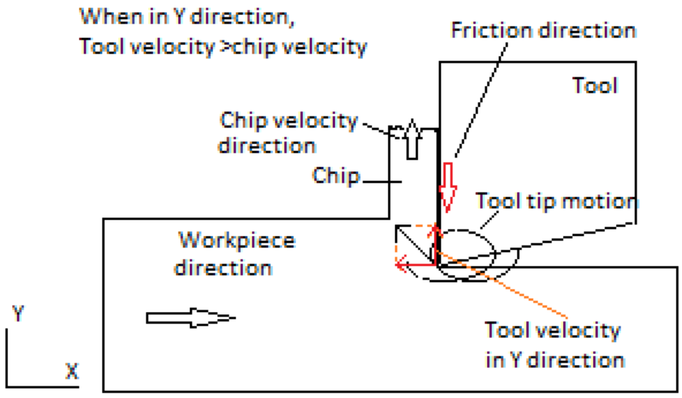

Fig. 4. 3 Schematic showing friction reversal

The time (t_r) at which this friction reversal takes place can obtained by following equation,

$$v_{tool-Y} \geq v_{chip-Y} \tag{4.1}$$

According to the continuity equation for conventional cutting, $v_{chip-Y} = v_{tool-X} \tan \Phi$, which can be further written as,

$$\omega b \sin \omega t_r \geq (a\omega \cos \omega t_r + v_{wkpc}) \times \tan \Phi \tag{4.2}$$

Where, φ is the shear angle at time(t_r) , v_{tool-Y} and v_{chip-Y} is the velocity component in Y direction for tool and chip respectively. For further explanation of this phenomenon one example is taken with cutting conditions: f=10 KHz, a=55 microns, b=20 microns, v_{wkpc}=0.1m/s and $\Phi = 40^\circ$ (shear angle varies in elliptical cutting but can be taken constant at a particular instant).

Based on these equations, velocity of chip and tool along Y-directions are shown in Fig.4.4

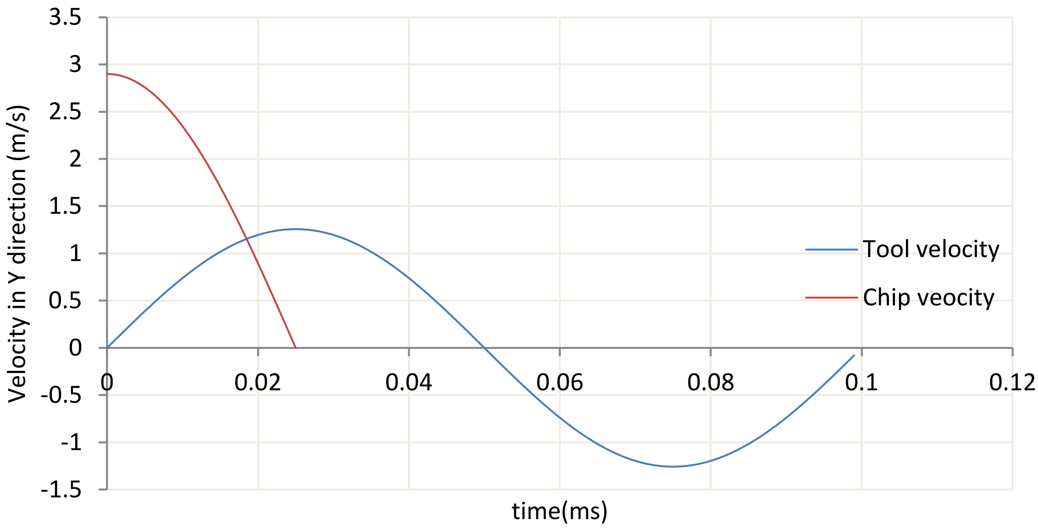

Fig. 4. 4 Variation of tool and chip velocity in Y direction

The FEA simulation also shows, Fig. 4.5, time of the reversal of friction which is matching with Fig..4.4.

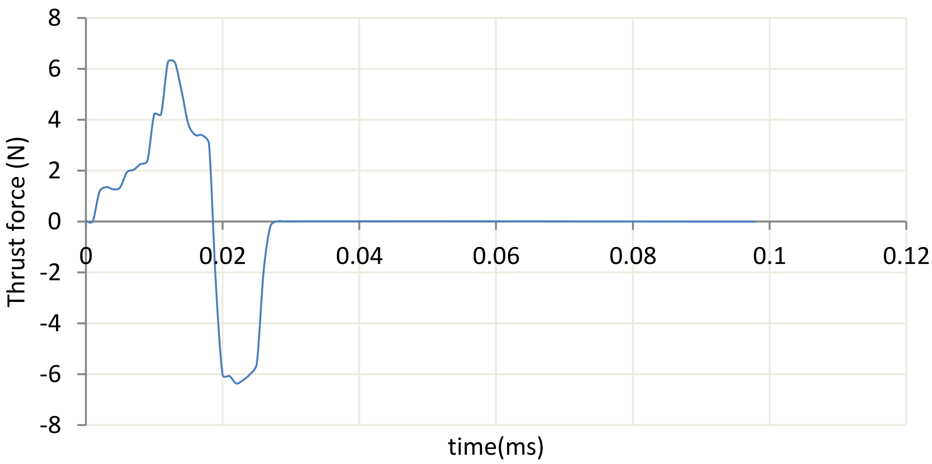

Fig. 4. 5 Simulation results of Thrust force variation during elliptical cutting

4.4 Cutting and thrust force variation during steady state

As one can see from the above Fig. 4.2 the values of the peak forces do not changes with time for elliptical cutting process although temperature values takes some time to reach steady state value. The steady state value of the cutting force is shown in the Fig. 4.6. As far as tool remains in contact with chip tool senses cutting force after that there are zero forces on the tool.

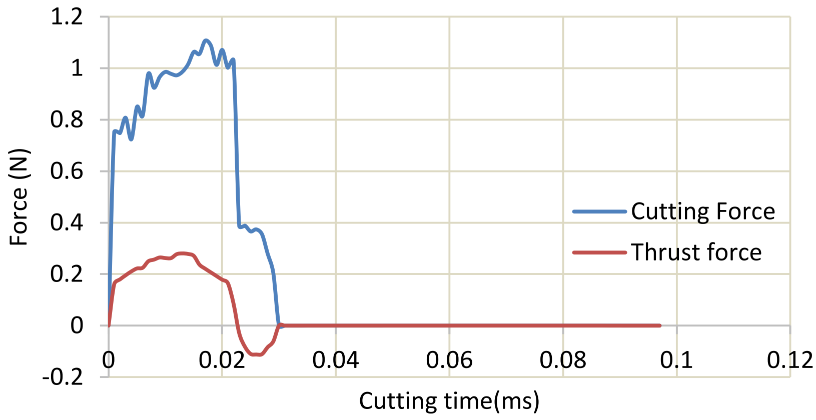

Fig. 4.6 Steady state variation in the Cutting and thrust forces during elliptical cutting, material AISI 1045 with SCD tool, cutting parameters: DOC: 2 micron, frequency: 10 KHz, ellipse amplitude: 11×2 micron

4.5 Tool tip temperature variation

Tool takes some time to reach steady state, under this state the heat coming from the chip and friction becomes equal to heat transferred to surroundings. The variation of the tool tip temperature with respect to time is shown in the Fig. 4.7.

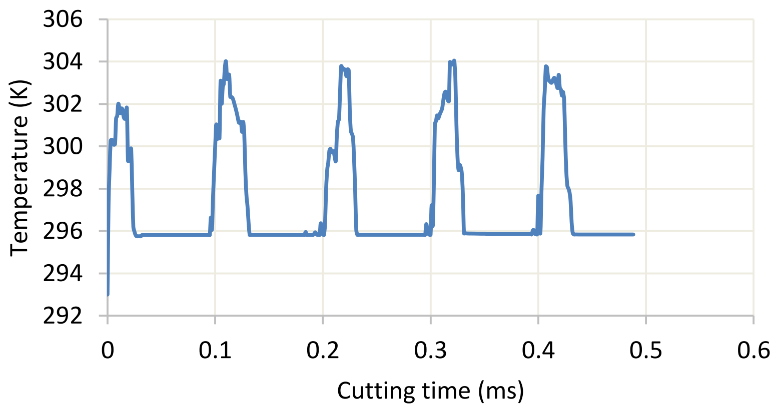

Fig. 4.7 Variation in the Tool tip temperature during elliptical cutting, material AISI 1045 with SCD tool, cutting parameters: DOC: 2 micron, frequency: 10 KHz, ellipse amplitude: 11×2 micron

4.6 Steady state tool tip temperature variation

In steady state peak and lowest temperature does not changes with new cutting cycle. The steady state temperature profile is shown in the Fig. 4.8..During contact time, the temperature increase at the tool tip, reaches maximum near the maximum uncut chip thickness zone and it comes down to residual value of temperature. The residual temperature/ non-contact time temperature remains almost constant.

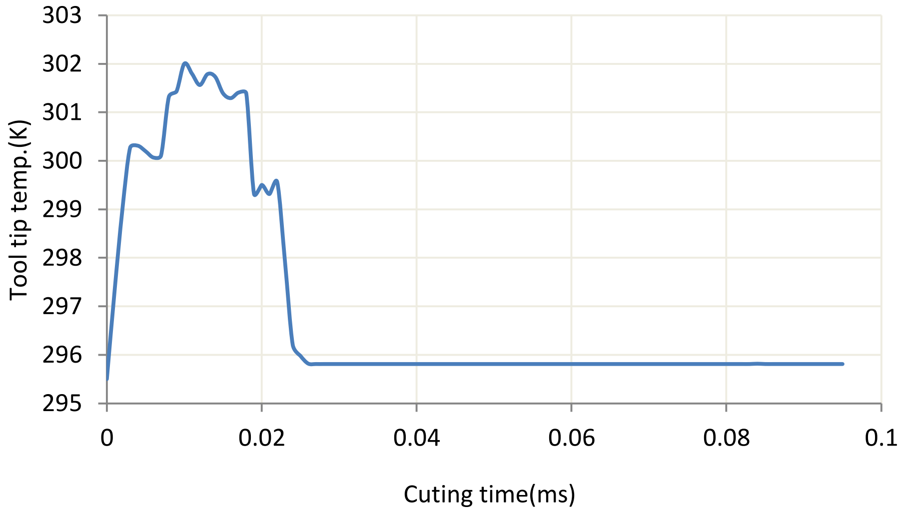

Fig. 4.8 Steady state cycle of the Tool tip temperature during elliptical cutting, material AISI 1045 with SCD tool, cutting parameters: DOC: 2 micron, frequency: 10 KHz, ellipse amplitude: 11×2 micron

Since the final steady state temperature and forces during cutting process are needed for the literature validation and understanding purpose, so form here onwards only steady state cycle data will be discussed in the chapter.

4.7 Literature validation

Validation of the FEA model of the elliptical cutting process can be done by simulating experimental results of elliptical cutting process using the experimental results taken from the literature [26]. The cutting conditions of the elliptical cutting used by the 2D elliptical cutting models are same as that used in the literature. The boundary conditions are taken as per cutting conditions in the simulations to give the near most results**.**

To validate the Arrhenius wear model for elliptical cutting tool wear predicted by simulation was compared with literature experimental values. Two values tool wear with cutting forces were compared with simulated values in cutting setup 1 and 2. The cutting conditions for experiment and simulation were kept similar.

4.7.1 Simulation cutting setup 1

The first cutting setup simulated with 1 KHz cutting frequency, $\mathbf{v_{wkpc}}$ = 2mm/s and a: 11micons and b: 2 microns .The simulated steady state cutting force and thrust force values are shown in the Fig. 4.9.The literature experimental result is shown in the Fig. B.2 in Appendix B. The two values are in well agreement with each other.

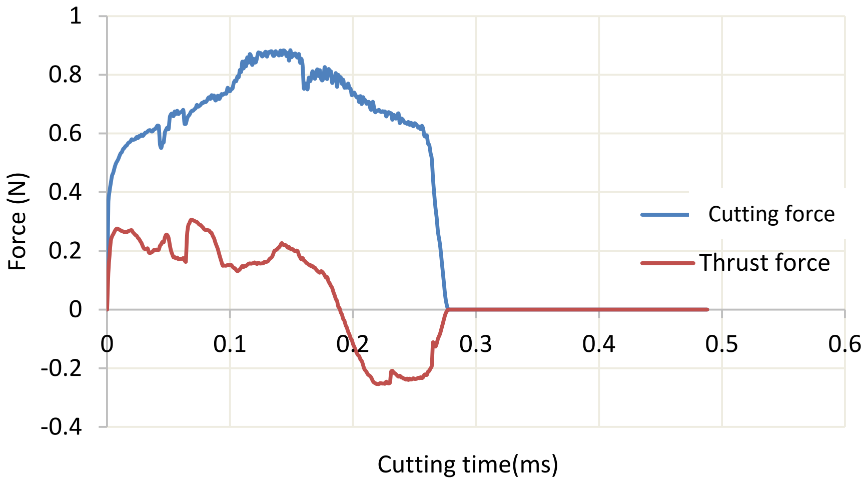

Fig. 4.9 Steady state variation in the Cutting and thrust forces during elliptical cutting, material AISI 1045 with SCD tool, cutting parameters: DOC: 2 micron, frequency: 1 KHz, ellipse amplitude: 11×2 micron

The simulated steady state temperature tool tip profile is shown in the Fig. 4.10**.** Since the cutting speed is very low the tool tip temperature is also very low the particular simulation.

Average temperature for contact time and whole cycle along with the conventional cutting temperature is compared in the Fig. 4.11. One can observe that the conventional cutting temperature is higher than the average temperature for the cycle. Till contact tool tip temperature is higher in elliptical cutting but during non-contact period the tool cools down and the overall cycle temperature reduces

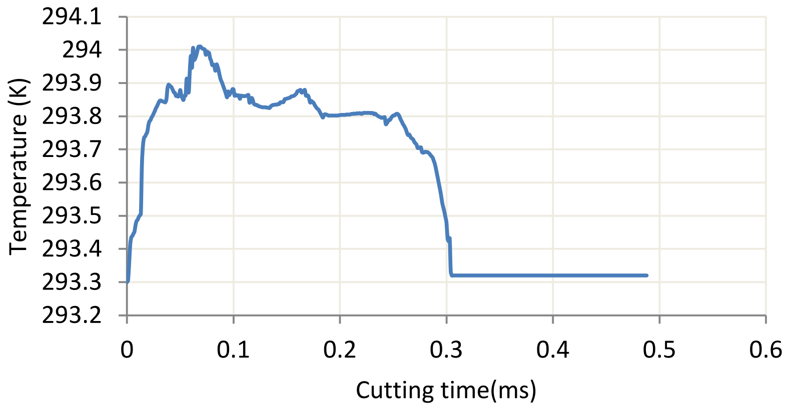

Fig. 4.10 Steady state cycle of the Tool tip temperature during elliptical cutting, material AISI 1045 with SCD tool, cutting parameters: DOC: 2 micron, frequency: 1 KHz, ellipse amplitude: 11×2 micron

. The values of tip temperature alone cannot represent the tool wear amount. The tool wear is calculated by evaluating the area under the curve given by equation A.7 from Appendix A, which is measured over the contact time period. So the Fig. 4.11 just shows the variation of the tool tip temperature over different time periods not of the tool wear. The Modulated average temperature over contact time is shown in the red color and can only be measured up to contact between tool and workpiece.

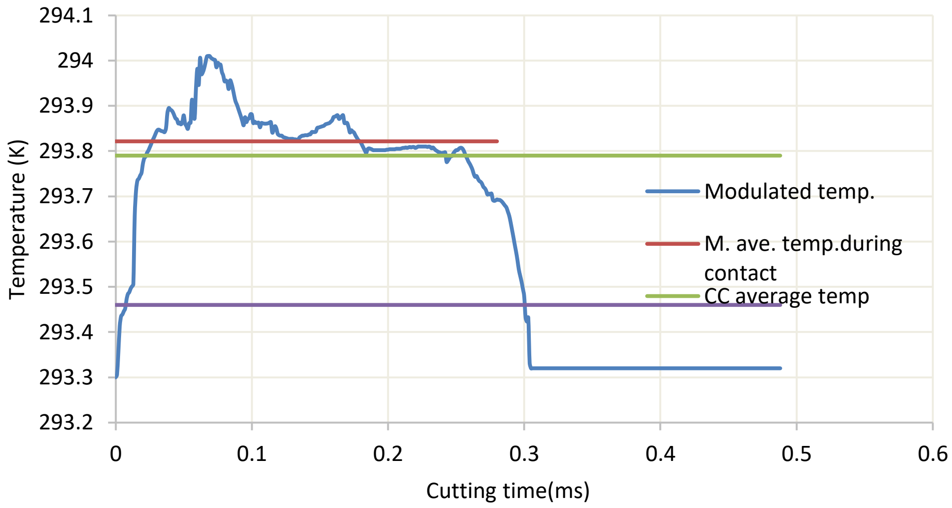

Fig. 4.11 Steady state cycle of the Tool tip temperature during elliptical cutting, material AISI 1045 with SCD tool, cutting parameters: DOC: 2 micron, frequency: 1 KHz, ellipse amplitude: 11×2 micron

A comparison of simulated tool wear rate and tool wear with the experiment values is shown in the Fig. 4.12. In bar chart (Fig. 4.12) simulated values of wear rate and wear for 5m cutting distances are compared with literature values respectively.

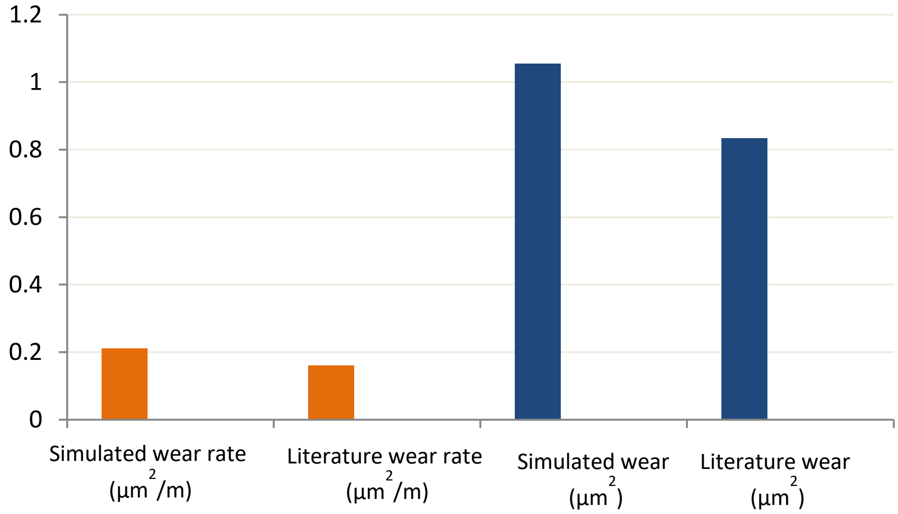

Fig. 4.12 Tool tip wear Simulated with Arrhenius model and its comparison with Actual measured wear. Cutting parameters: DOC: 2 micron, frequency: 1 KHz, ellipse amplitude: 11×2 micron

The blue color bar shows the wear rate and orange color bar shows tool wear amount. The values predicted by the simulation shows the deviation within 26 % of the literature values. The variation in results may have risen due to various assumptions taken for the FEA analysis

4.7.2 Simulation cutting setup 2

The second cutting setup simulated with 2 KHz cutting frequency, $\mathbf{v_{wkpc}}$= 4mm/s and a: 11micons and b: 2 microns**.** The variation of the cutting and thrust force observed is shown in the Fig. 4.13.The thrust force takes a dip as negative value due friction force reversal. The maximum value of the cutting force did not changed much with respect to the 1KHz condition as the cutting forces majorly depends upon the uncut chip geometry.

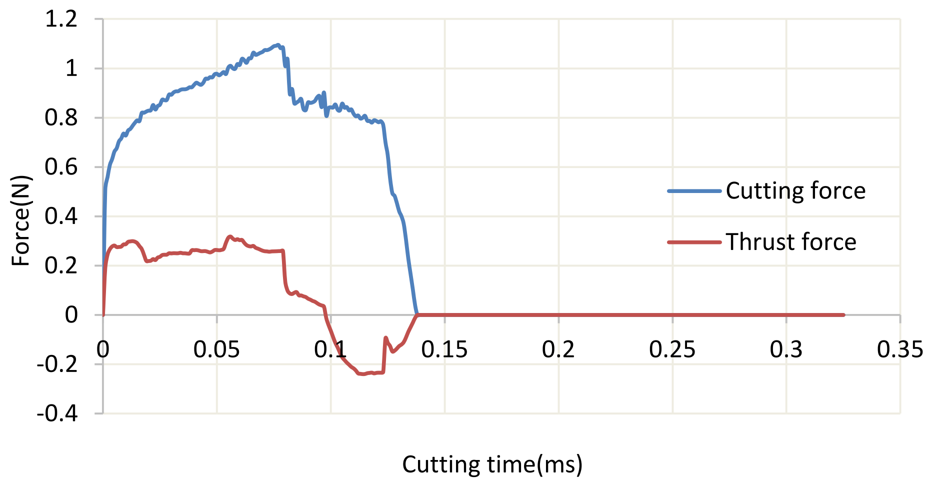

Fig. 4.13 Steady state variation in the Cutting and thrust forces during elliptical cutting, material AISI 1045 with SCD tool, cutting parameters: DOC: 2 micron, frequency: 2 KHz, ellipse amplitude: 11×2 micron

The literature experimental values of the cutting force measured from the cutting are shown in the Fig. B.3 in Appendix B. The peak value of the cutting force is around 1 N which as predicted by the FEA model. Since the experimental setup for force possesses limitations of data points measured par second, the resolution of the forces measured is also gets limited by this.

The steady state tool tip temperature generated during cutting at 2 KHz is shown in the Fig. 4.14. The peak temperature is increased due to high cutting velocities compared to 1 KHz cutting model. The comparison of the different cutting temperatures for single cutting cycle is shown in the Fig. 4.15.The average value of modulated temperature for a cycle is lower than the average temperature in the conventional cutting which supports the claims from the literature. On the other hand the peak temperature and average temperature up to contact in higher in elliptical cutting process.

The tool wear calculated with the help of equation A.9 from Appendix A and experimentally measured values are shown in the Fig. 4.16. The predicted tool wear and wear rate are in agreement (< 21% deviation) with the literature values but some deviation may be seen form results due to the assumptions made during the FEA modeling.

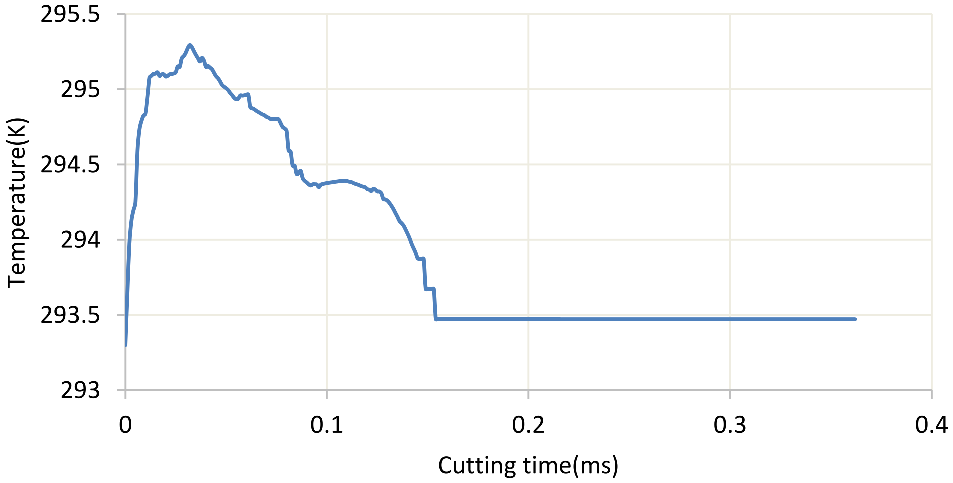

Fig. 4.14 Steady state cycle of the Tool tip temperature during elliptical cutting, material AISI 1045 with SCD tool, cutting parameters: DOC: 2 micron, frequency: 2 KHz, ellipse amplitude: 11×2 micron

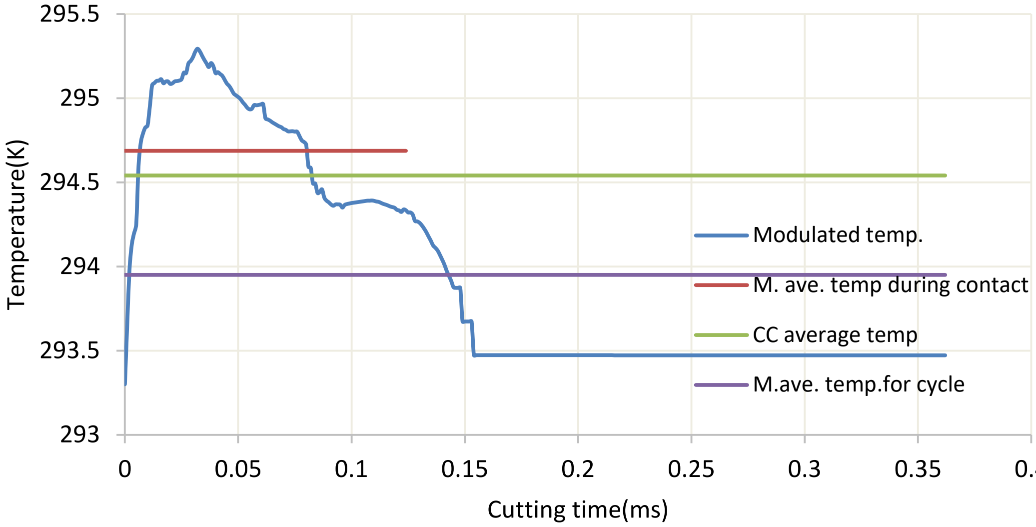

Fig. 4.15 Steady state cycle of the Tool tip temperature during elliptical cutting, material AISI 1045 with SCD tool, cutting parameters: DOC: 2 micron, frequency: 2 KHz, ellipse amplitude: 11×2 micron

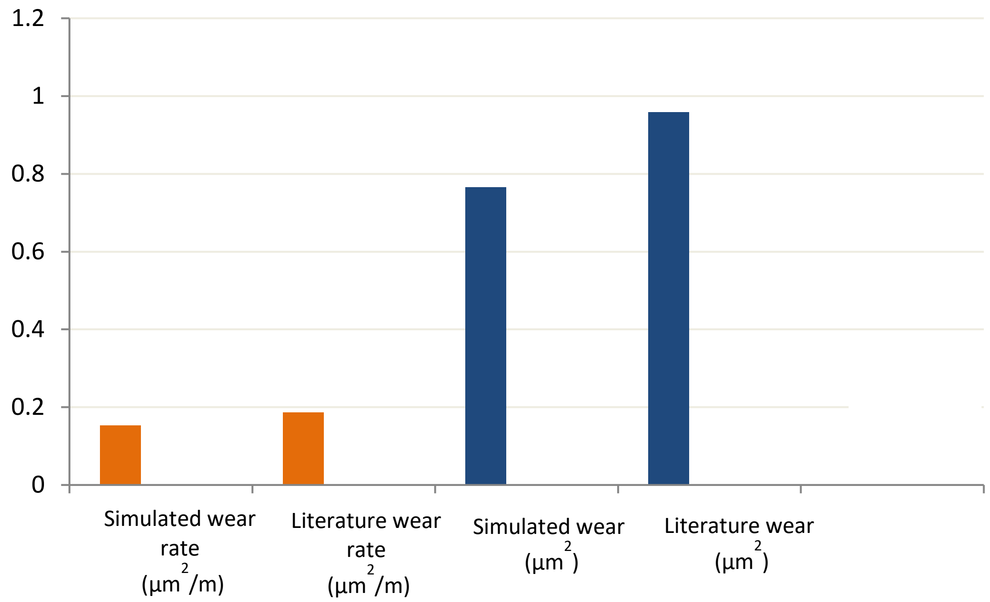

Fig. 4.16 Tool tip wear simulated with Arrhenius model and its comparison with literature wear. Cutting parameters: DOC: 2 micron, frequency: 2 KHz, ellipse amplitude: 11×2 micron

The tool wear reported by literature predicts lower and higher tool wear for 1 KHz and 2 KHz cutting frequencies as compared to simulation results as shown in the Fig. 4.12 and 4.16 respectively. This variation can be explained with the help of other sources of tool wear, acting in experimental conditions and was not incorporated in this simulation model. Diffusion and Impact wear in the cutting process also plays minor role in tool wear and can cause deviation from the simulation results. The main factors influencing these wear are

i. Diffusion wear: Temperature acts as main parameter for affecting wear rate.
ii. Impact wear (tool tip breakage): Sudden jerks on the tool tip affect this wear rate.

Diffusion of carbon atoms into freshly generated steel surface is a temperature dependent phenomenon [8]. In the presence of high cutting stresses at the tool tip with temperature increase the carbon atoms disassociate from the tool surface and diffuses into the interstitial sites of iron lattice at elevated temperature (as the workpiece temperature is much higher than the tool tip). The temperature at tool tip and workpiece for 2 KHz cutting frequency is higher, which can cause more tool wear. So the experimental results shows relatively higher tool wears for 2 KHz cutting frequency. Along with this, Impact wear can cause the breakage of tool tip of the hundreds of nanometres order along the cutting edge due to sudden jerk created at the time of tool and workpiece contact. Higher the contact velocity higher the chances and degree of the impact wear. Those two factors combined may cause variation between experimental and simulation values which leads to higher experimental wear than the predicted simulation wear.

Chapter 5
Optimization of elliptical cutting process

5.1 Introduction

The literature survey and chapter 4 shows that the tool wear during elliptical cutting depends upon variouaus cutting parameters. Elliptical cutting contains a large number of machining parameters which further complicates there effect on the tool wear. To better understand the effect of different cutting parameter like cutting frequency, workpiece speed, HSR, ellipse amplitudes, contact time, tool tip velocity etc. on the tool wear this chapter contains a series of FEA simulations while changing the important cutting parameters. Contact time during elliptical cutting process affect tool wear since it governs the extent of the chemical tool wear reaction or graphitization. To better understand this effect the variation of tool wear with contact time is shown during different cutting parameters. Cutting forces generated during machining process depends upon process parameters and amount of tool wear at tool tip. This tool wear may occur at flank or rake face of the tool. The cutting forces on the tool depends upon the tool wear and changes with amount of tool wear. Although for this study the effect on the tool wear on the cutting forces is out of scope but these outcomes may work as reference for the future study purpose.

5.2 Simulation setup

Simulation time for attaining steady state in elliptical cutting process becomes very high for smaller depth of cuts like 1 or 2 microns due to smaller elements size. To increase the number of simulations for elliptical cutting process with available computation power the simulation mode size was increased to 10 times. The bigger model takes lesser simulation time for a single simulation so more number of FEA simulations could be conducted for better understanding of the process. The results produced by bigger model will follow the same temperature and force trend but the values will be higher. The depth of cut for all simulations was kept constant. The value of the Arrhenius equation coefficients for the simulations were taken as E_a=29.3 KJ/mol and A=329$\mu m^2/s$ and kept same for all simulations. To see the effect of contact time on the tool wear in better way the simulations were done by changing a few parameters while keeping others constant at a time. The simulations were done by changing the frequency, amplitude, HSR and amplitude & frequency while keeping other parameters constant each time. Further, values of the tool tip temperature and cutting forces were analyzed with respect to contact time in absolute and relative wear terms. Absolute terms represent to true function of EVAM, and relative terms are more appropriate for modeling purposes.

5.3 Frequency variation

The frequency of elliptical cutting was changed while keeping the up feed per cycle (upfc) constant. In this way sliding distance and chip area removed in each cycle is equal and do not changes with frequency change.

Table 5.1 Cutting conditions for frequency variation

EVAM frequency	4, 10, 20, 40,60, 80 KHz
Ellipse shape	55×20 microns
Depth of cut	40 microns
Work piece velocity	0.04, 0.1, 0.2, 0.4, 0.6, 0.8 m/s
Tool Material	Single crystal diamond
Work piece material	1045 steel

5.3.1 Results

The variation of the cutting forces during cutting with process parameters as per Table 1 as shown in Fig. 5.1. Cutting force and Thrust force both of the forces are shown in the variation. Since the uncut chip shape for each of these simulations is the same and the only parameter that varies is velocity, the tool forces in the EVAM simulations vary little with frequency.

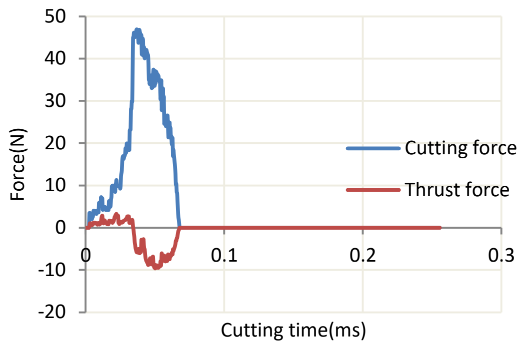

(a) f-4KHz

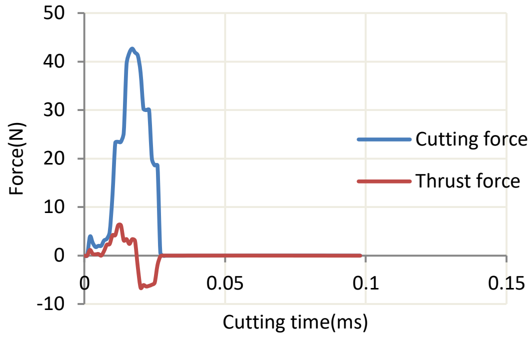

(b) f-10KHz

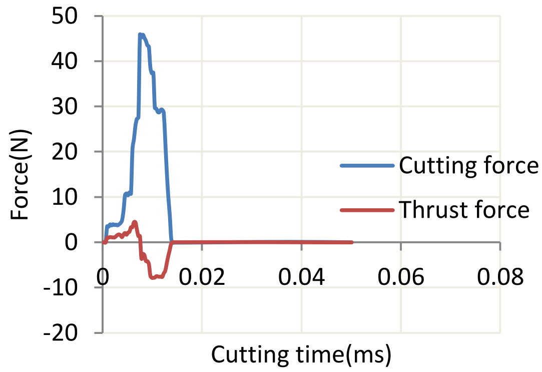

(c) f-20KHz

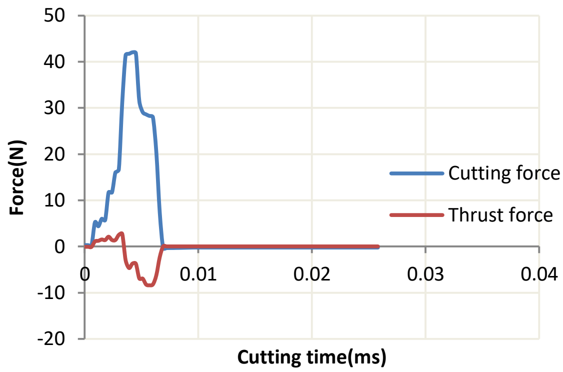

(d) f-40KHz

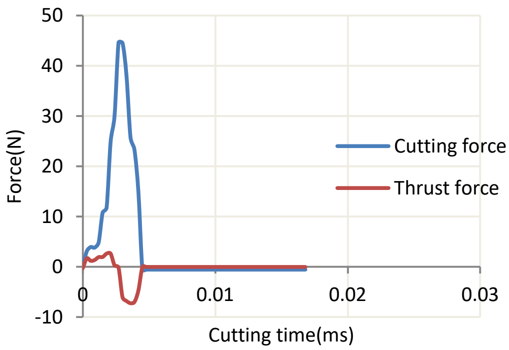

(e) f-60KHz

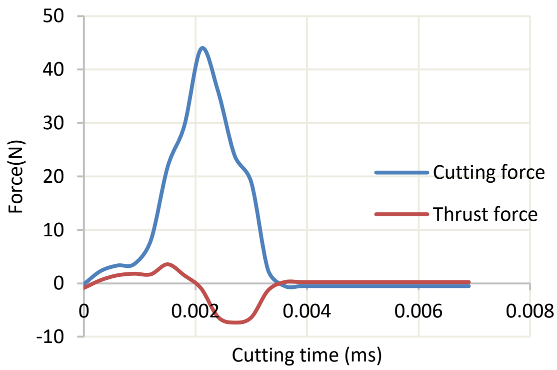

(f) f-80KHz

Fig. 5.1 Variation in Cutting and thrust force from (a) to (f) with various frequencies, Tool: SCD and Work piece material: 1045 steel

The variation in the tool tip temperature during cutting process with cutting conditions as par table 5.1 is shown the Fig. 5.2.

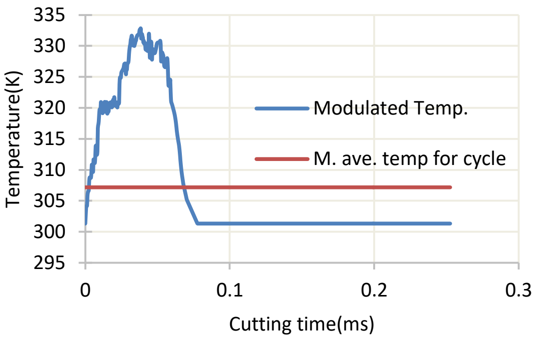

(a) f-4KHz

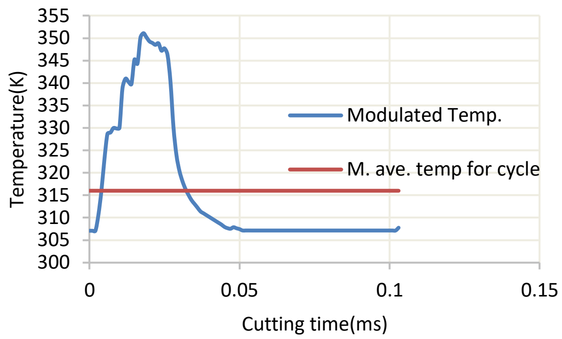

(b) f-10KHz

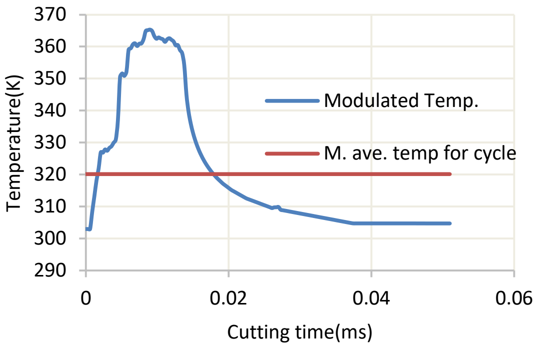

(c) f-20KHz

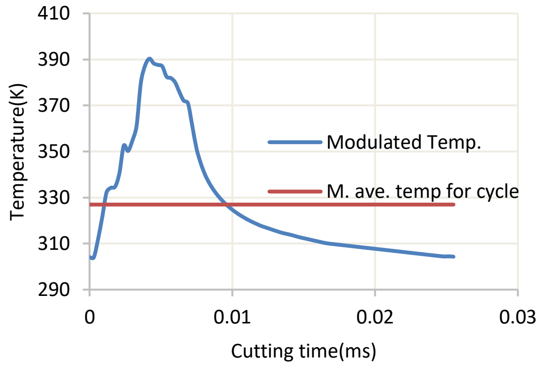

(d) f-40KHz

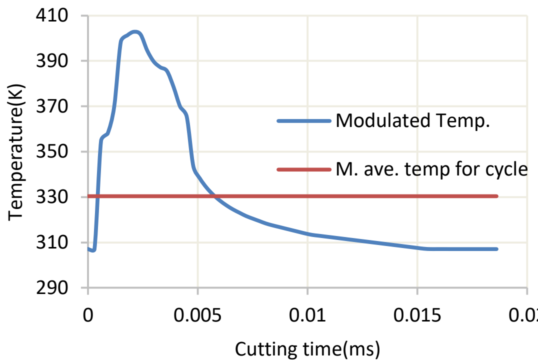

(e) f-60KHz

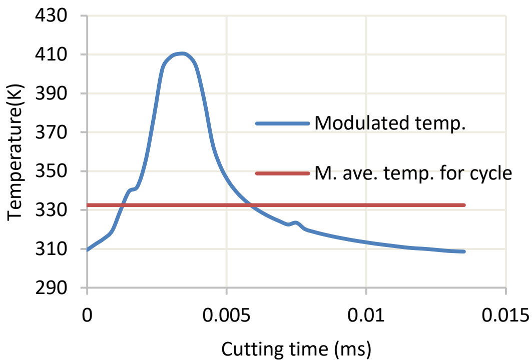

(f) f-80KHz

Fig. 5.2 Variation in Tool tip temperature from (a) to (f) with various Frequencies, Tool: SCD and Work piece material: 1045 steel

Since the tool tip temperature depends upon on the tool's cutting velocity so its value increases with increase in tool tip velocity. As the linear frequency of the cutting is increased the tool tip velocity increases and cooling time reduces, both of the factors increases the tool tip temperature. The Fig. 5.2 also shows the average temperature for the modulated cycle.

Average temperature can be used to compare the heat transferred to the tool tip which is responsible to chemical tool wear.

Fig. 5.3 shows the tool wear per unit machining distance as the linear frequency increase. Form the graph it is clear that as the frequency increases the tool wear reduces in terms of machining distance. This shows that the tool can cut for longer distances for the same amount of wear as the frequency is increased while keeping chip geometry unchanged.

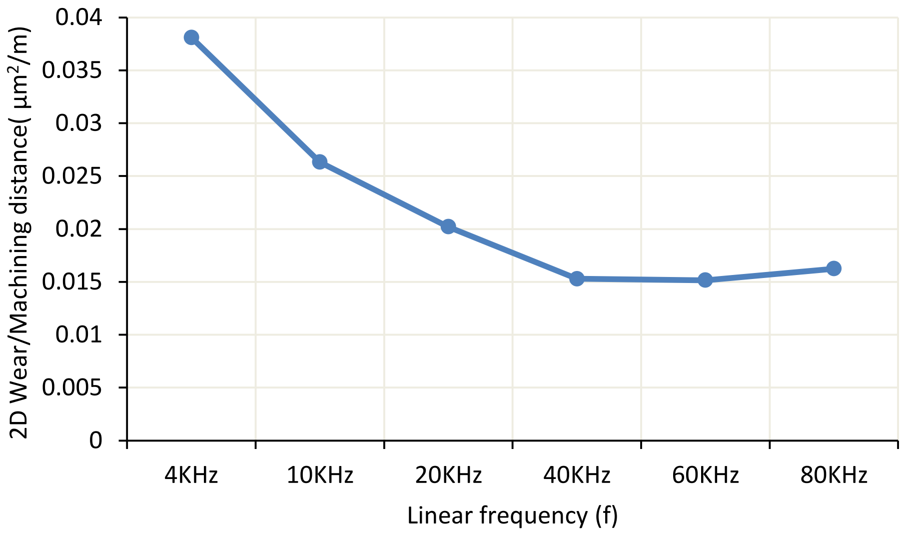

Fig. 5.3 Wear rate for increase in linear frequency of elliptical cutting Tool: SCD and Work piece material: 1045 steel, Cutting conditions: Table 5.1

Table 5.2 shows the value of the Contact time for various linear frequencies while keeping the cutting parameters as Table 5**.**1**.**Contact time between tool tip and chip can be evaluated with the equation shown in Appendix A.

Table 5.2 Linear frequency and their corresponding contact times

Linear frequency	**Contact time (ms)**
4 KHz	6.6E-02
10 KHz	2.64E-02
20 KHz	1.32E-02
40 KHz	6.6E-02
60 KHz	4.4E-02
80 KHz	3.3E-02

Form the Table 5.2; it is clear that the contact time reduces as the cutting frequency increases while keeping ellipse amplitude constant. The variation of the tool tip temperature with contact time is shown in the Fig. 5.4; it is evident form the graph that the tool wear reduces with reduction in the contact time, although the average tool tip temperature increases. It shows that there exist two significant factors for chemical tool wear (graphitization reactions):

i. Tool tip temperature
ii. Contact time

Since the contact time plays an important role in the chemical wear reaction, the wear reduces with reduction in the contact time. In the frequency variation simulation tool temperature increases with increase in frequency on the other hand contact time reduces simultaneously. The increase in temperature increases the wear rate and reduction in contact time reduces wear rate with increase in frequency. So two significant factors acts in opposite manner and their relative dominance defines the minimum value in the wear rate. It can also be seen from the graph that before minima reduction in contact time is dominant (since wear rate is reducing), while after tool tip temperature becomes dominant (Since wear rate is increasing). Fig. 5.5 shows the variation of the wear with unit sliding distance, which helps to understand the intrinsic behavior of the wear. This shows that the tool wear increases with increase in the contact time i.e. higher the contact time higher the time for chemical wear process.

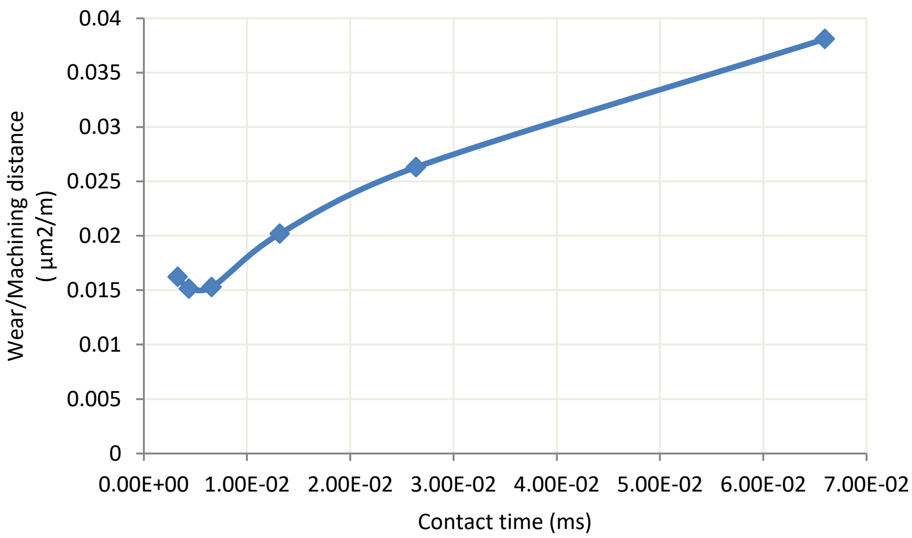

Fig. 5.4 Wear rate corresponding to various contact time (reducing) of elliptical cutting Tool: SCD and Work piece material: 1045 steel, Cutting conditions: Table 5.1

Although there exists a point before which this effect may get reversed but this occurs at relatively very high cutting frequency i.e. around 60 KHz to 80 KHz [47]. So during major practical portion of cutting frequencies, increase in contact time also increases the wear.

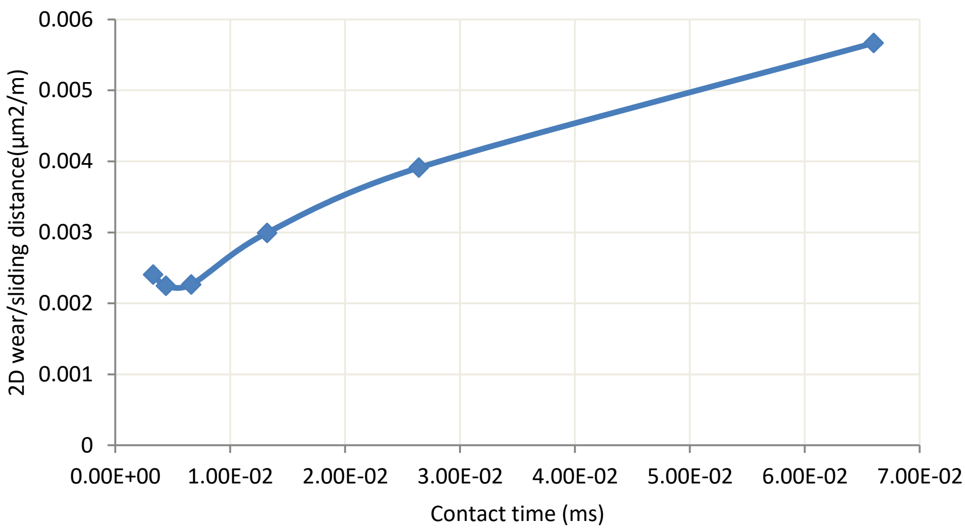

Fig. 5.5 Wear rate (relative parameters) corresponding to various contact time of elliptical cutting Tool: SCD and Work piece material: 1045 steel, Cutting conditions: Table 5.1

The wear rate (relative parameters) decreases with increase in contact time for high frequency/lower contact time values but after a minima point, it increases with increase in contact time. The point of minima appears at very high linear frequencies or when the contact time is lesser.

5.4 HSR variation

High speed ratio is an important cutting parameter in elliptical cutting, since horizontal speed ratio (HSR) relates the peak EVAM ellipse speed to the work piece velocity. As the HSR varies, the area of chip removed and contact time also varies, which in turn control the wear rate.

The Table 5.4 shows the HSR and contact time corresponding to the different work piece cutting velocities.

Table 5.3 HSR variation parameters

EVAM frequency	10 KHz
Ellipse shape	55×20 microns
Depth of cut	40 microns
Work piece velocity	0.1, 0.2, 0.6, 1.0 m/s
Tool Material	Single crystal diamond
Work piece material	1045 steel

As the workpiece velocity increases HSR also increases since the maximum absolute tool tip velocity is kept constant.

Table 5.4 HSR and Contact time for various work piece velocities

Work piece velocity (v_{wkpc} m/s)	**HSR**	**Contact time (ms)**
0.1	0.028129	2.64E-02
0.2	0.054718	2.77E-02
0.6	0.147962	3.27E-02
1.0	0.224462	3.75E-02

5.4.1 Results

Fig. 5.6 shows the variation of the cutting forces with change in the workpiece velocity or HSR. The cutting forces increases with increase in the workpiece cutting velocity as the uncut chip area also increases with it, higher the resistance from the material higher the cutting forces in the tool.

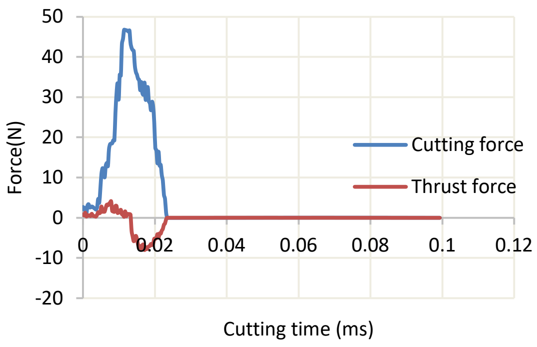

(a) f-10KHz, v-0.1m/s

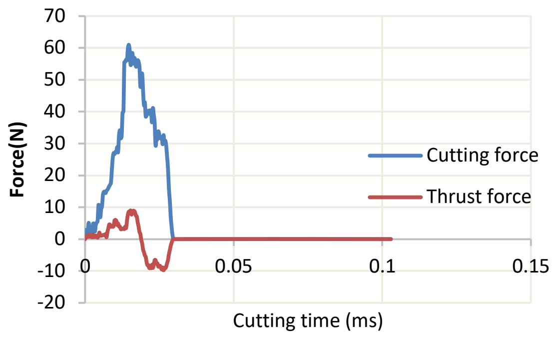

(b) f-10KHz, v-0.2m/s

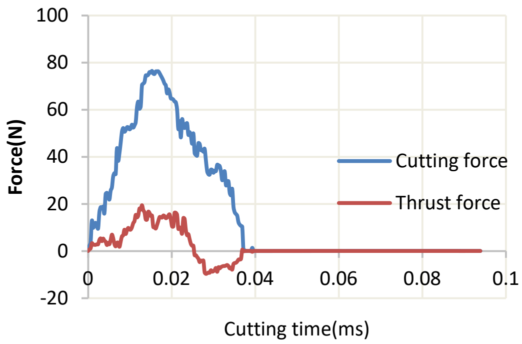

(c) f-10KHz, v- 0.6m/s

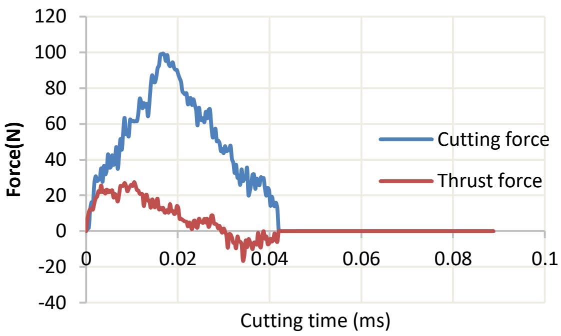

(d) f-10KHz, v-1m/s

Fig. 5.6 Variation in Cutting and thrust force from (a) to (d) with various HSR, Tool: SCD and Work piece material: 1045 steel, Cutting conditions: Table 5.3

Fig. 5.7 shows the tool tip temperature variation with variation in the workpiece velocity or HSR. The tool tip temperature increases with increases in the workpiece velocity due to more uncut chip area.

The relative wear rate increases with increase in the HSR, so as the workpiece velocity increases the tool wear at faster rate as shown in the Fig. 5.8.

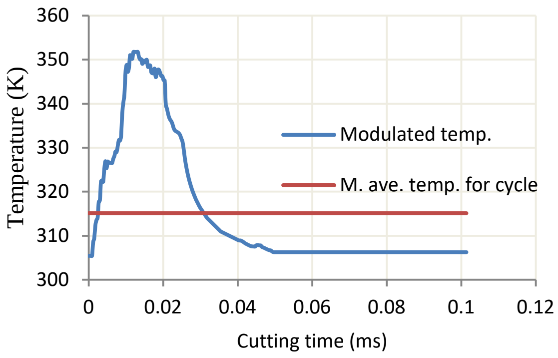

(a) f-10KHz, v-0.1m/s

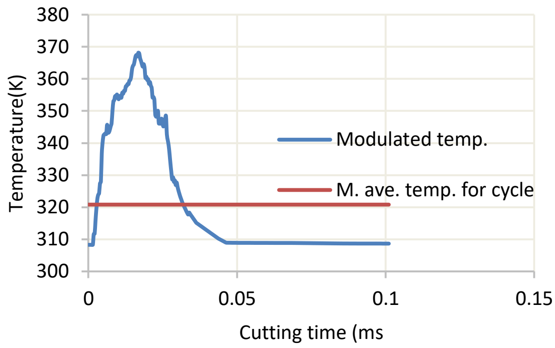

(b) f-10KHz, v-0.2m/s

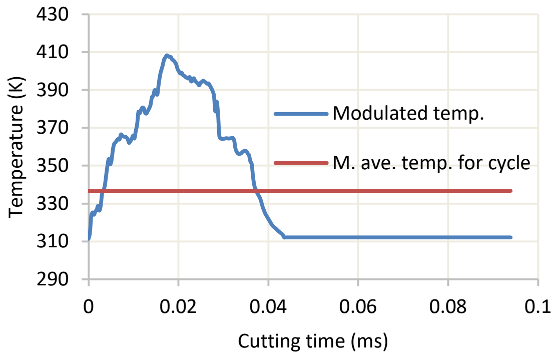

(c) f-10KHz, v-0.6m/s

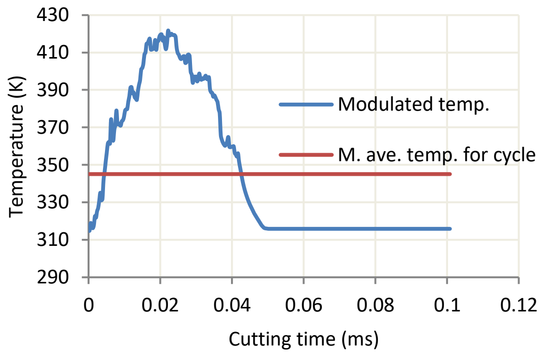

(d) f-10KHz, v-1m/s

Fig. 5.7 Variation in Tool tip temperature from (a) to (d) with various HSR, Tool: SCD and Work piece material: 1045 steel, Cutting conditions: Table 5.3

Fig. 5.9 shows that the relative tool wear rate increases with increases in the contact time similar to the previous observations. The contact time corresponding to each HSR value is shown in the Table 5.4. Fig. 5.10 shows the wear per unit machining distance variation for the contact time variation corresponding to HSR variation. Wear per unit machining distance reduces with increase in the contact time due to spread of the tool wear over longer cutting distances

Spreading of the tool wear occurs due increase in the workpiece velocity spreads the same amount of tool wear over longer machining distances.

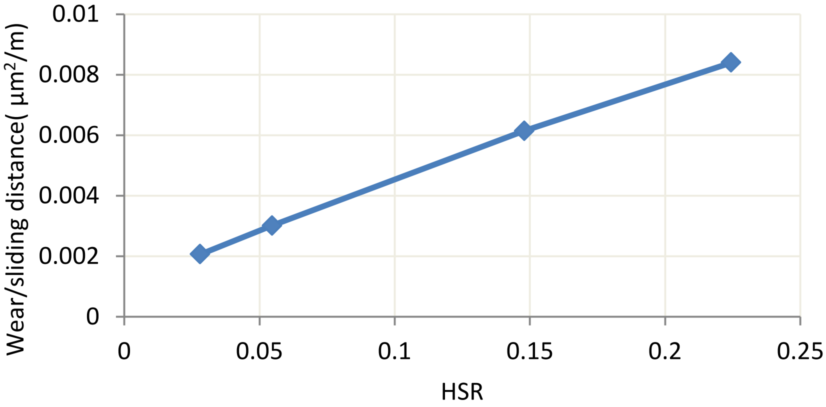

Fig. 5.8 Wear rate for increase in HSR of elliptical cutting Tool: SCD and Work piece material: 1045 steel, Cutting conditions: Table 5.3

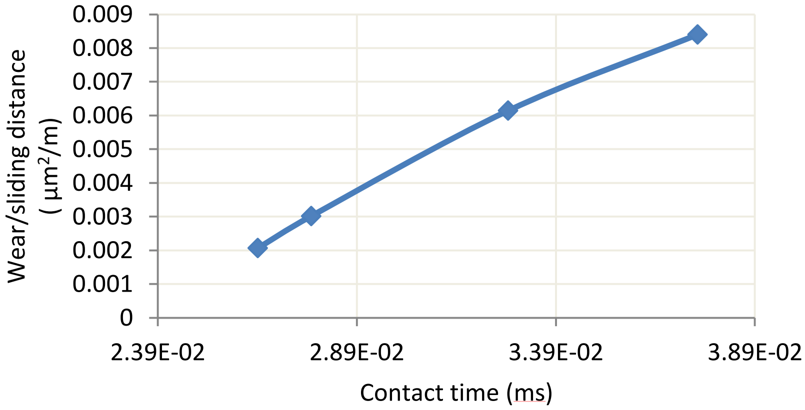

Fig. 5.9 Wear rate (relative parameters) corresponding to various contact time of elliptical cutting Tool: SCD and Work piece material: 1045 steel, Cutting conditions: Table 5.3

The result form Fig. 5.9 shows tool wear rate when the tool is in contact with the work piece while the Fig. 5.10 shows the total machined distance by the tool over the work piece. The amount of wear produced in a single slide (cycle) can be distributed over different machined distances and it depends upon size, shape, frequency and work piece velocity.

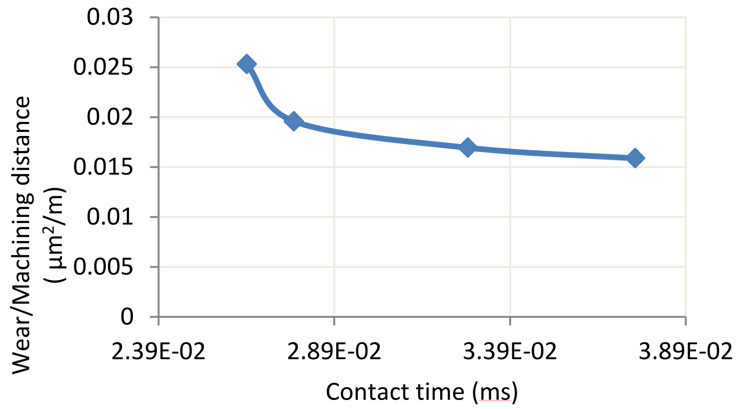

Fig. 5.10 Wear rate corresponding to various contact time of elliptical cutting Tool: SCD and Work piece material: 1045 steel, Cutting conditions: Table 5.3

Some observations worth notice are as follows:

i. Wear rate (relative parameters) increases with increase in contact time.

ii. Although wear per unit machining distance decreases with increase in contact time due to higher increase in the r_{up}, than the wear rate (wear/sliding distance).

5.5 Amplitude variation

The effect of amplitude ratio (a/b) on the wear rate can be observed by comparing the wear rate for horizontal, circular and vertical ellipse. This will also show which ellipse shape is better for elliptical cutting.

Table 5.5 Cutting conditions for amplitude variation

EVAM frequency	20 KHz
Ellipse shape	56.6×11.3, 25 × 25, 11.3×56.6 microns
Ellipse aspect ratio	5.01, 1.00, 0.02
Depth of cut	40 microns
Work piece velocity	0.237, 0.07, 0.02m/s
Tool Material	Single crystal diamond
Work piece material	1045 steel

The ellipse shape is based upon 'a' and 'b' amplitudes values. The Horizontal, vertical and circular ellipse and there amplitudes are shown in the table 5.6

Table 5.6 Contact time for amplitude variation

Conditions (a μm× b μm)	**Elliptic path**	**Contact time (ms)**
56.6×11.3	Horizontal	1.33E-02
25.3× 25.3	Circular	1.3E-02
11.3×56.6	Vertical	1.28E-02

5.5.1 Results

The variation of the cutting forces with horizontal, circular and vertical elliptic tool tip path is shown in the Fig. 5.11. The horizontal elliptic path produces highest cutting forces due to larger uncut chip area.

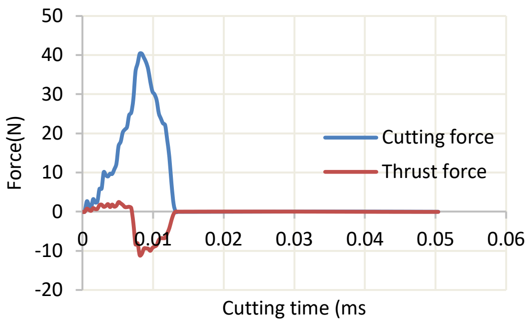

(a) 25 μm ×25μm

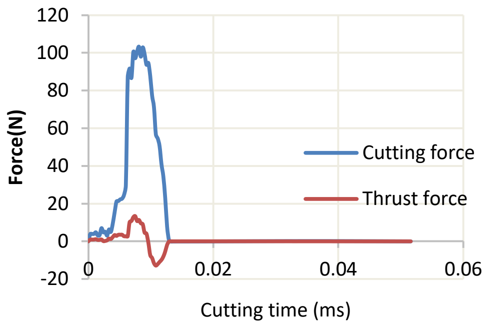

(b) 55 μm ×11 μm

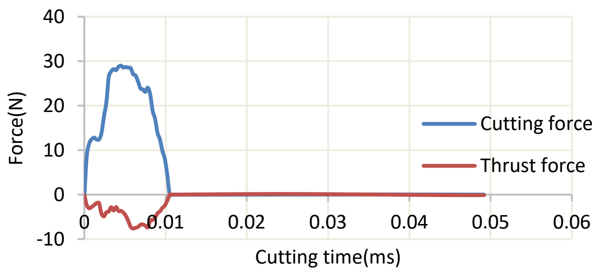

(c) 11.3μm×56.6μm

Fig. 5.11 Variation in Cutting and thrust force from (a) to (c) with various ellipse aspect ratios, Tool: SCD and Work piece material: 1045 steel, Cutting conditions: Table 5.5

The Fig. 5.12 shows the variation of the cutting temperature with different elliptic tool paths.

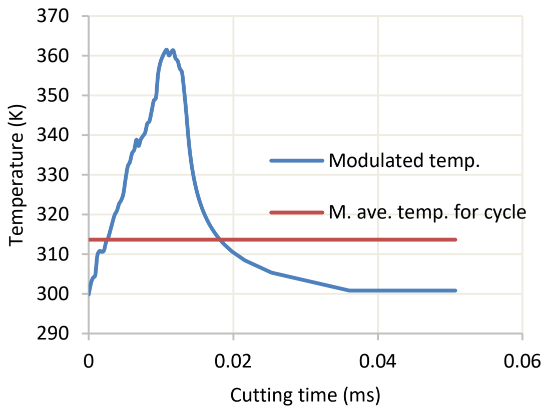

(a) 25 µm ×25µm

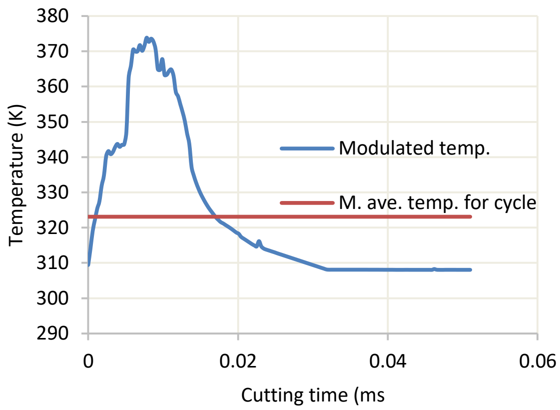

(b) 55 µm ×11 µm

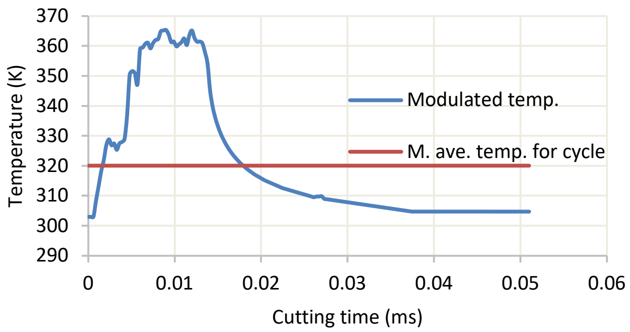

(c) 11.3µm×56.6µm

Fig. 5.12 Variation in Tool tip temperature from (a) to (c) with Ellipse aspect ratios, Tool: SCD and Work piece material: 1045 steel, Cutting conditions: Table 5.5

The horizontal elliptic tool path generates higher tool tip temperature and cutting forces but due to wear got spread longer distances the wear per unit machining distance turns out to be lower for horizontal ellipse as shown in the Fig. 5.13.

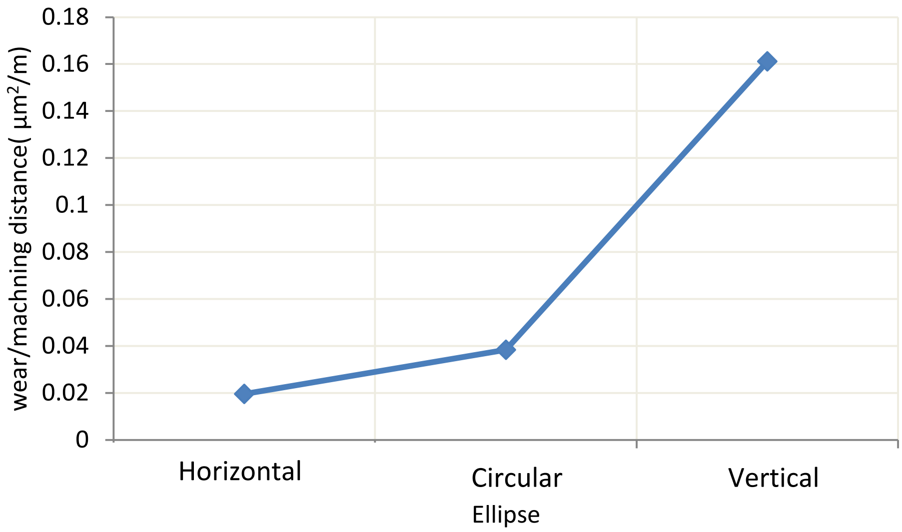

Fig. 5.13 Wear rate corresponding to Ellipse shape Tool: SCD and Work piece material: 1045 steel, Cutting conditions: Table 5.5

The horizontal elliptic path causes higher tool wear in the tool due higher contact time and temperature over the unit sliding distance. The minimum tool wear is caused by the vertical elliptic tool paths as shown in the Fig. 5.14.

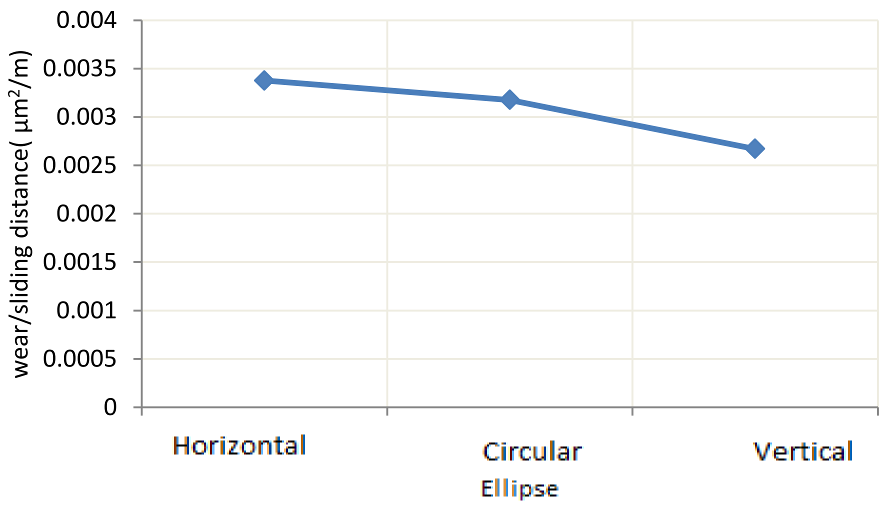

Fig. 5.14 Wear rate (relative parameters) corresponding to Ellipse shape Tool: SCD and Work piece material: 1045 steel, Cutting conditions: Table 5.5

Corresponding contact time for amplitude change is shown in the Fig. 5.15.The relative wear increases with increases in the contact time.

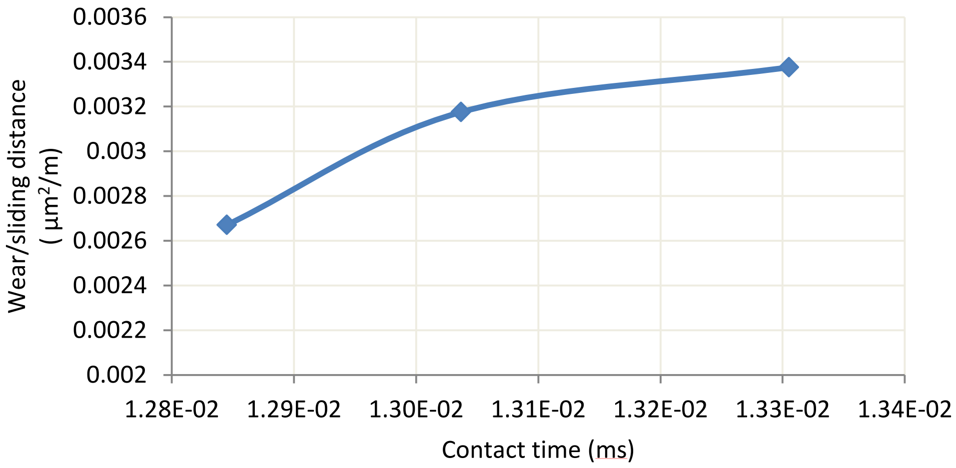

Fig. 5.15 Wear rate (relative parameters) corresponding to varying contact time Tool: SCD and Work piece material: 1045 steel, Cutting conditions: Table 5.5

Some points worth notice are as following:

i. With increase in contact time wear/sliding distance increases.
ii. Horizontal ellipse gives lower tool wear for a particular machining distance. Although the wear/sliding distance is more in horizontal ellipse. This is due to "spreading of wear" for longer machining distance.

5.6 Amplitude and frequency variation

Frequency was increased by factor of two, while horizontal amplitude was decreased by a factor of two to result in the simulation parameters in Table 5.7. Work piece velocity is kept constant for each simulation.

Table 5.7 Cutting conditions for Amplitude and frequency variation

EVAM frequency	10, 20, 40 KHz
Ellipse shape	110×20, 55 × 20, 22.5×20 microns
Depth of cut	40 microns
Work piece velocity	0.2m/s
Tool Material	Single crystal diamond
Work piece material	1045 steel

Table 5.8 Contact time for frequency and amplitude variation

Conditions (f KHz, a μm ×b μm)	**Contact time (ms)**
Case I- 10KHz, 110×20	2.64E-02
Case II- 20KHz, 55×20	1.32E-02
Case III- 40KHz, 22.5×20	6.68E-03

5.6.1 Results

Forces were higher for the low frequency, large amplitude simulation due to the larger 2D uncut chip area and thickness as shown in the Fig. 5.16.

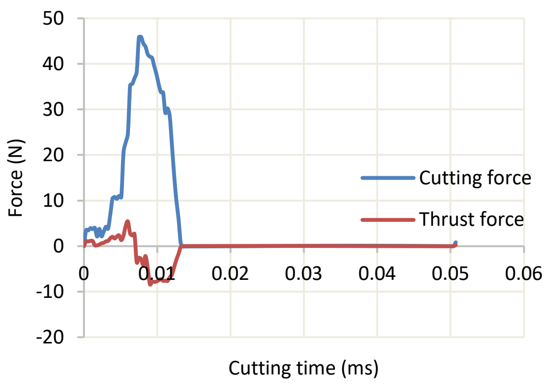

(a) f-20KHz, 55 μm ×20μm

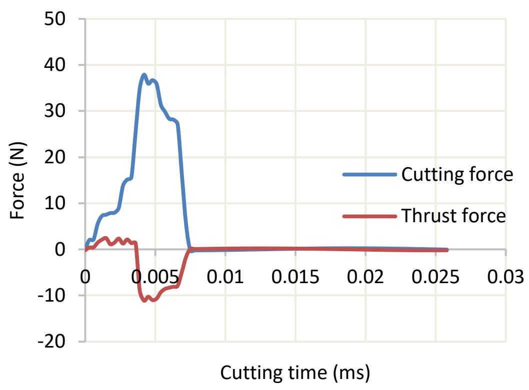

(b) f-40KHz-22.5 μm ×20 μm

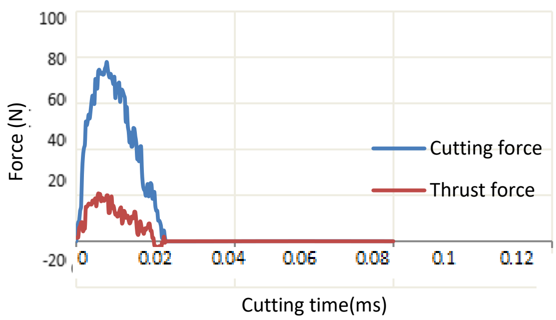

(c) f-10KHz, 110 μm ×20 μm

Fig. 5.16 Variation in Cutting and thrust force from (a) to (c) with Frequency and amplitude, Tool: SCD and Work piece material: 1045 steel, Cutting conditions: Table 6

The Fig. 5.17 shows that the higher frequency cut generates higher tool tip temperature due to higher strain rate.

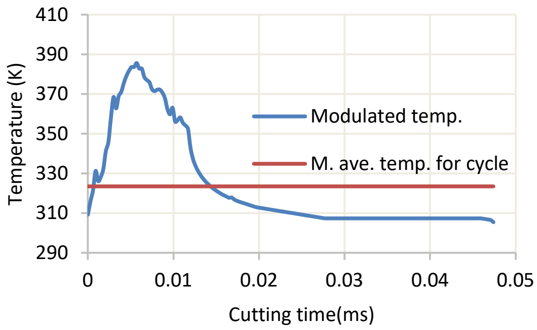

(a) f-20KHz, 55 µm ×20µm

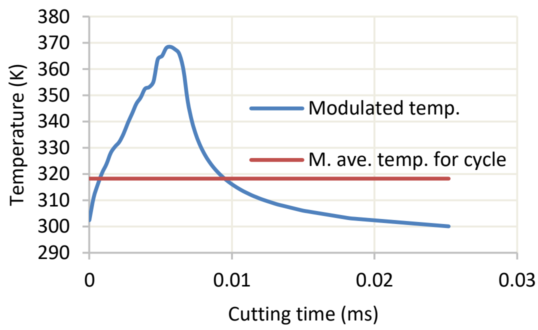

(b) f-40KHz-22.5 µm ×20 µm

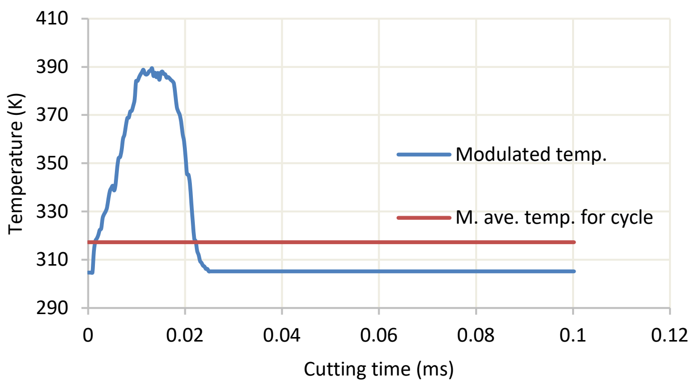

(c) f-10KHz, 110 µm ×20 µm

Fig. 5.17 Variation in Tool tip temperature from (a) to (c) with Frequency and amplitude, Tool: SCD and Work piece material: 1045 steel, Cutting conditions: Table 5.7

The variations in the tool wear with respect to change in frequency and amplitude simultaneously is shown in the Fig. 5.18. The overall effect of these two parameters depends upon the combination of the cutting frequency and amplitude values.

The variation in the wear/sliding distances with corresponding contact time for table 5.7 cutting conditions are shown in the Fig. 5.19. As the contact time increases the wear/machining distance value also increases.

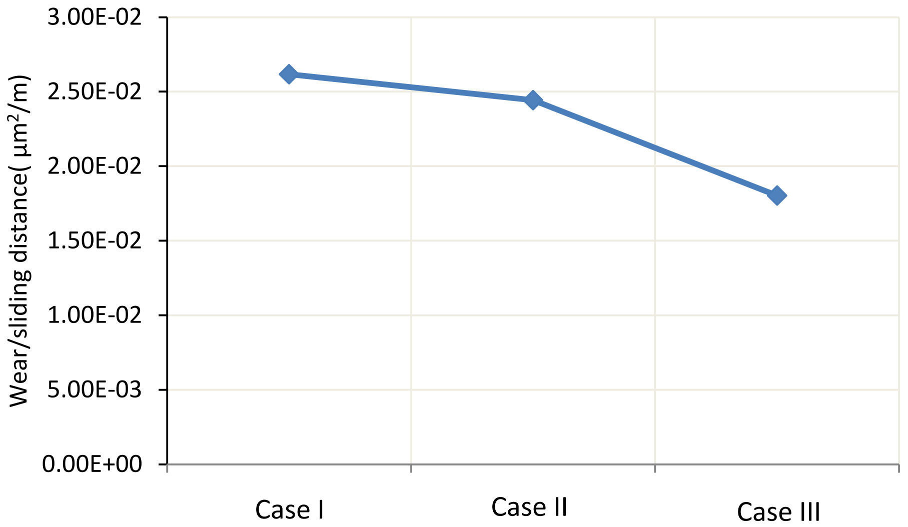

Fig. 5.18 Wear rate (relative parameters) corresponding to varying frequency and amplitude, Tool: SCD and Work piece material: 1045 steel, Cutting conditions: Table 5.7

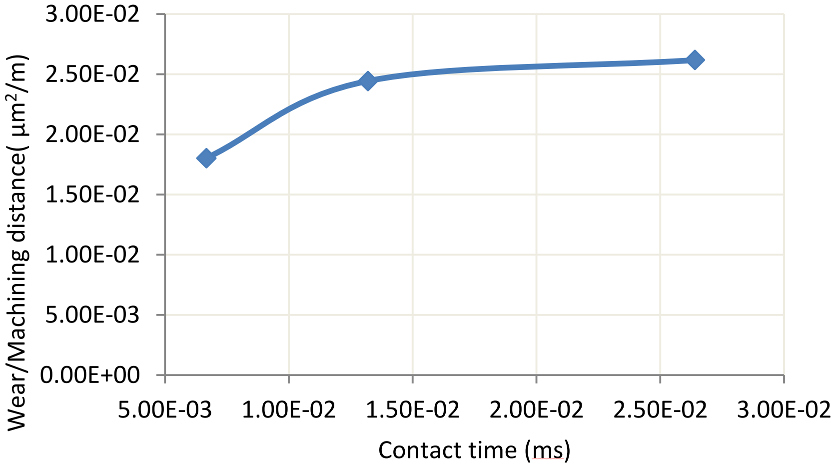

Fig. 5.19 Wear rate corresponding to varying contact time Tool: SCD and Work piece material: 1045 steel, Cutting conditions: Table 5.7

Fig. 5.20 shows that the relative wear increases with increase in the contact time.

Some points worth notice are as following:

i. With increase in contact time wear/sliding distance increases.
ii. Combined effect of frequency and amplitude decides overall impact on the tool wear rate.

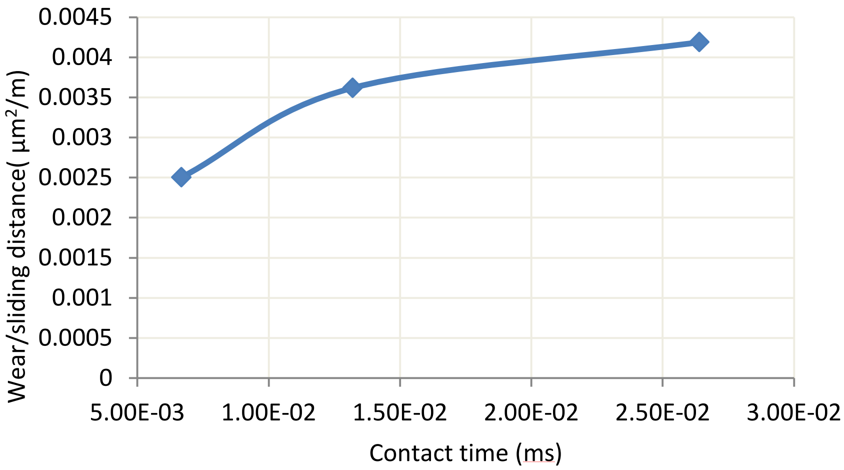

Fig. 5.20 Wear rate (relative parameters) corresponding to varying contact time Tool: SCD and Work piece material: 1045 steel, Cutting conditions: Table 5.7

The varying uncut chip shapes and chip thicknesses do not allow a simple comparison to the Arrhenius wear model. The simulations sets with varying frequency, HSR, ellipse shape, and combined frequency and amplitude help to understand the trends that can optimize ECM in terms of reducing wear. Relative tool wear rate helps to better understand the effect of contact time between tool and work piece compare to absolute wear rate (gives wear over machined distance of work piece). It is an important observation that the relative tool wear in the simulations shows a similar trend with contact time. As the contact time of tool tip with work piece increases the relative tool wear rate also increases. Although absolute wear rate may increase or decrease depending upon the up- feed ratio. As the contact time increases tool wear also increases (shown by relative tool wear) but the spreading of tool wear over machining distance (shown by absolute wear) may increase or decrease depending upon the up feed ratio. In the variation with frequency simulation one can also observe a minimum value of tool wear corresponding to a contact time. Contact time and cutting velocity play an important role in chemical wear along with tool tip temperature. The simulation set that varied frequency maintained constant uncut chip shapes simplify the process and shows the effect of contact time on the tool wear in clearer way. The simulations conducted in this chapter provide insights which are useful for better understanding of diamond tool wear during elliptical cutting process.

The simulations for cutting forces variations show that cutting forces mostly depends on the shape and area of the uncut chip (in 2D profile). As the chip area depends upon the upfc and

DoC of the uncut chip. In all the simulations it is seen that the cutting forces increases with increase in upfc since tool has to remove more material. The change in cutting velocity has little or no effect on the peak cutting forces as shown in Fig. 5.1. Preferably, in the condition of frequency changing, the peak cutting forces do not change with time given no tool wear conditions. Since the cutting forces also depend on the tool tip geometry, these forces will change with the amount of tool wear at flank or rake face [48]. So these cutting conditions along with a force measuring system can be used to predict diamond tool wear with respect to tool wear during elliptical cutting.

Chapter 6
Conclusion and Future work

6.1 Conclusion

In this study numerical investigation on the 2D Modulated cutting machining/elliptical cutting was conducted. The FEA model for the chemical tool wears i.e. Arrhenius tool wear model was used to model the single crystal diamond tool wear while cutting ferrous metal i.e. AISI 1045. In the elliptical cutting process the contact time between tool and freshly formed surface after machining plays an important role in tool wear and can be used for tool wear minimization. FEA simulations were done while changing the elliptical cutting parameters in defined manner. Some conclusion worth noticeable are mentioned below:

1. A numerical diamond tool wear model via finite element analysis was generated to imitate the SCD tool wear in conventional cutting process. Later the model was modified to predict the diamond tool wear in case of elliptical cutting processes.
2. Diamond tool wear process during cutting of ferrous materials followed the Arrhenius tool wear equation. This point support the claim that SCD tool wear while cutting ferrous materials is dominantly chemical in nature and can be predicted with proper wear constants.
3. The value of average tool tip temperature for a cycle in elliptical cutting process is less as compared to conventional cutting process due to cooling effect in non-contact period and reduced chip thickness.
4. Horizontal ellipse showed less wear/ machining distance compared to vertical and circular path although wear/sliding distances were high. This shows horizontal ellipse spreads the tool wear over more cutting distances.

5. Contact time plays an important role in chemical wear process along with tool tip temperature and the statement can be backed by the results showed in chapter 5. Results shows that as the contact time in elliptical cutting process increase the tool wear rate (relative tool wear) also increases for the major practical frequency range.
6. In the elliptical cutting process with frequency increase, there exist minima for tool wear as the contact time reduces while keeping the uncut chip shape and other parameters constant.

6.2 Future work

1. FEA analysis conducted by the researchers generally neglects the effect of the continuous deterioration of tool tip sharpness as it does in actual experiments. Thus to ensure better results a FEA model with tool tip wear feedback values can be established.
2. A practical method for actual temperature measurement can be established for concrete understanding of tool tip temperature variation in elliptical cutting process.
3. One generalized model for diamond tool wear can be generated including other wear mechanism like diffusion, oxidation and there weightage in the diamond tool wear along with graphitization wear.
4. The cutting forces on the tool wear changes with amount of tool wear and can be used to create a real time system for tool wear tracking.

References

1. Balasubramaniam, R., Sarepaka, R.V., & Subbiah, S. (2017). Diamond Turn Machining: Theory and Practice (1st ed.) CRC Press.

2. Field, J.E., 2012. The mechanical and strength properties of diamond. Reports on Progress in Physics, 75(12), 126505.

3. Irifune, T., Kurio, A., Sakamoto, S., Inoue, T. and Sumiya, H., 2003. Ultrahard polycrystalline diamond from graphite. Nature, 421(6923), 599-600.

4. Gogotsi, Y.G., Kailer, A. and Nickel, K.G., 1999. Transformation of diamond to graphite. Nature, 401(6754), 663-664.

5. Thornton, A.G. and Wilks, J., 1978. Clean surface reactions between diamond and steel. Nature, 274(5673), 792-793.

6. Uemura, M., 2004. An analysis of the catalysis of Fe, Ni or Co on the wear of diamonds. Tribology International, 37(11-12), 887-892.

7. Chacham, H. and Kleinman, L., 2000. Instabilities in diamond under high shear stress. Physical review letters, 85(23), 4904.

8 Zou, L., Yin, J., Huang, Y. and Zhou, M., 2018. Essential causes for tool wear of single crystal diamond in ultra-precision cutting of ferrous metals. Diamond and Related Materials, 86, 29-40.

10. Paul, E., Evans, C.J., Mangamelli, A., McGlauflin, M.L. and Polvani, R.S., 1996. Chemical aspects of tool wear in single point diamond turning. Precision Engineering, 18(1), 4-19.

11. Shimada, S., Tanaka, H., Higuchi, M., Yamaguchi, T., Honda, S. and Obata, K., 2004. Thermo-chemical wear mechanism of diamond tool in machining of ferrous metals. CIRP Annals, 53(1), 57-60.

12. Uemura, M., 2004. An analysis of the catalysis of Fe, Ni or Co on the wear of diamonds. Tribology International, 37(11-12), 887-892.

13. Zou, L., Yin, J., Huang, Y. and Zhou, M., 2018. Essential causes for tool wear of single crystal diamond in ultra-precision cutting of ferrous metals. Diamond and Related Materials, 86, 29-40.

14. Wang, Y., Suzuki, N., Shamoto, E. and Zhao, Q., 2011. Investigation of tool wear suppression in ultraprecision diamond machining of die steel. Precision engineering, 35(4), 677-685.

15. Moriwaki, T. and Shamoto, E., 1991. Ultraprecision diamond turning of stainless steel by applying ultrasonic vibration. CIRP Annals, 40(1), 559-562.

16 Shamoto, E. and Moriwaki, T., 1999. Ultaprecision diamond cutting of hardened steel by applying elliptical vibration cutting. CIRP Annals, 48(1), 441-444.

17. Brinksmeier, E. and Gläbe, R., 2001. Advances in precision machining of steel. CIRP Annals, 50(1), 385-388.

18. ZHANG, J., 2014. Micro/Nano machining of steel and tungsten carbide utilizing elliptical vibration cutting technology (Doctoral dissertation, Nagoya University)

19. Zhang, Y., Zhou, Z., Lv, Y., Wang, J., Shao, L. and Iqbal, A., 2013. Wear behavior of natural diamond tool in cutting tungsten-based alloy. The International Journal of Advanced Manufacturing Technology, 69(1-4), 329-335.

20. Ma, C., Shamoto, E., Moriwaki, T. and Wang, L., 2004. Study of machining accuracy in ultrasonic elliptical vibration cutting. International Journal of Machine Tools and Manufacture, 44(12-13), 1305-1310.

21. Nath, C., Rahman, M. and Neo, K.S., 2009. A study on the effect of tool nose radius in ultrasonic elliptical vibration cutting of tungsten carbide. Journal of Materials Processing Technology, 209(17), 5830-5836.

22. Liu, X.D., Ding, X., Lee, L.C., Fang, F.Z. and Lim, G.C., 2003, October. Direct single point diamond cutting of stavax assisted with ultrasonic vibration to produce optical quality surface finish. In ASPE Proceedings 2003 Annual Meeting (67-70).

23. Bulla, B., Klocke, F., Dambon, O. and Hünten, M., 2012. Ultrasonic assisted diamond turning of hardened steel for mould manufacturing. In Key Engineering Materials (Vol. 516, 437-442). Trans Tech Publications Ltd.

24. Klocke, F., Dambon, O. and Bulla, B., 2011. Tooling system for diamond turning of hardened steel moulds with aspheric or non rotational symmetrical geometries. In Proceedings of the 11th International Euspen Conference, Como, Italy.

25. Bulla, B., Klocke, F., Dambon, O. and Hünten, M., 2012. Ultrasonic assisted diamond turning of hardened steel for mould manufacturing. In Key Engineering Materials (Vol. 516, 437-442). Trans Tech Publications Ltd.

26. Lane, B., 2012. Material Effects and Tool Wear in Vibration Assisted Machining. Mechanical Engineering, North Carolina State University, Raleigh, North Carolina.

27. Patten, J.A. and Williams, A., 2013. Numerical simulations of vibration assisted machining. Manufacturing Research Center Western Michigan University Kalamazoo, Michigan.

28. Song, Y., Nezu, K., Park, C.H. and Moriwaki, T., 2009. Tool wear control in single-crystal diamond cutting of steel by using the ultra-intermittent cutting method. International Journal of Machine Tools and Manufacture, 49(3-4), 339-343.

29. Chen, H., Cheng, M., Li, Y. and Zhang, D., 2011. Development of integrated precision vibration-assisted micro-engraving system. Transactions of Tianjin University, 17(4), 242-247.

30. Brinksmeier, E. and Gläbe, R., 2001. Advances in precision machining of steel. CIRP Annals, 50(1), 385-388.

31. Paul, E., Evans, C.J., Mangamelli, A., McGlauflin, M.L. and Polvani, R.S., 1996. Chemical aspects of tool wear in single point diamond turning. Precision Engineering, 18(1), 4-19.

32. Zareena, A.R. and Veldhuis, S.C., 2012. Tool wear mechanisms and tool life enhancement in ultra-precision machining of titanium. Journal of Materials Processing Technology, 212(3), 560-570.

33. Tanaka, H., Shimada, S., Higuchi, M., Yamaguchi, T., Kaneeda, T. and Obata, K., 2005. Mechanism of cutting edge chipping and its suppression in diamond turning of copper. CIRP Annals, 54(1), 51-54

34. Wilks, E.M. and Wilks, J., 1972. The resistance of diamond to abrasion. Journal of Physics D: Applied Physics, 5(10), 1902.

35. Brinksmeier, E., Gläbe, R. and Osmer, J., 2006. Ultra-precision diamond cutting of steel molds. CIRP Annals, 55(1), 551-554.

36. Wang, Y., Suzuki, N., Shamoto, E. and Zhao, Q., 2011. Investigation of tool wear suppression in ultraprecision diamond machining of die steel. Precision engineering, 35(4), 677-685.

37. Marksberry, P.W. and Jawahir, I.S., 2008. A comprehensive tool-wear/tool-life performance model in the evaluation of NDM (near dry machining) for sustainable manufacturing. International Journal of Machine Tools and Manufacture, 48(7-8), 878-886.

38. Archard, J., 1953. Contact and rubbing of flat surfaces. Journal of applied physics, 24(8), 981-988.

39. Lane, B., 2010. Development of Predictive Models for Abrasive and Chemical Wear of Diamond Tools. Mechanical and Aerospace Engineering, North Carolina State University, Raleigh, North Carolina.

40. Uemura, M., 2004. An analysis of the catalysis of Fe, Ni or Co on the wear of diamonds. Tribology International, 37(11-12), 887-892.

41. He, Y., Zou, P., Zhu, W.L. and Ehmann, K.F., 2017. Ultrasonic elliptical vibration cutting of hard materials: simulation and experimental study. The International Journal of Advanced Manufacturing Technology, 91(1), 363-374.

42. Lane, B.M., Dow, T.A. and Scattergood, R., 2013. Thermo-chemical wear model and worn tool shapes for single-crystal diamond tools cutting steel. Wear, 300(1-2), 216-224.

43. Yoshino, M., Nakajima, S. and Terano, M., 2015. Tool wear of a single-crystal diamond tool in nano-groove machining of a quartz glass plate. Surface Topography: Metrology and Properties, 3(4), 044007.

44. Johnson, G.R., 1983. A constitutive model and data for materials subjected to large strains, high strain rates, and high temperatures. Proc. 7th Inf. Sympo. Ballistics, 541-547.

45. Shamoto, E. and Suzuki, N., 2014. Ultrasonic vibration diamond cutting and ultrasonic elliptical vibration cutting. PY: 2014/05/01, SP405, EP454, VL11, DO10.1016/B978-0-08-096532-1.01111-0, JO: Comprehensive Materials Processing.

46. Borsos, B., Csörgő, A., Hidas, A., Kotnyek, B., Szabó, A., Kossa, A. and Stépán, G., 2017. Two-dimensional finite element analysis of turning processes. Periodica Polytechnica Mechanical Engineering, 61(1), 44-54.

47. Zhang, S.J., To, S. and Zhang, G.Q., 2017. Diamond tool wear in ultra-precision machining. The International Journal of Advanced Manufacturing Technology, 88(1), 613-641.

48. Lane, B.M., Shi, M., Dow, T.A. and Scattergood, R., 2010. Diamond tool wear when machining Al6061 and 1215 steel. Wear, 268(11-12), 1434-1441.

Appendix A

i. EVAM Nomenclature and Tool wear calculations

a, b are ellipse horizontal and vertical amplitude, respectfully (1/2 of major and minor axis of the ellipse), *DoC* is Depth of cut, distance from part surface to lowest point of ellipse, v_{wp} is workpiece velocity with respect to ellipse centre, ω is EVAM frequency in radians per second, f is EVAM frequency in cycles per second.

Ufpc is up-feed per cycle, the distance the centre of the ellipse travels in one EVAM cycle.

$$ufpc = \frac{v_{wkpc}}{f} \tag{A.1}$$

HSR is horizontal speed ratio, ratio of the workpiece velocity to the maximum tangential velocity of the ellipse.

$$HSR = \frac{v_{wkpc}}{a\omega} \tag{A.2}$$

α_{min} is minimum tool clearance angle, *ds* is sliding distance per cycle, calculated by section of tool trajectory which the tool is in contact with workpiece, r_{up} is sliding distance per upfeed ratio, ratio of ds to ufpc which can be multiplied by total cut distance to total sliding distance, Chip area is always equivalent to upfc×DoC

Critical time points are, T: EVAM cycle period, t_0: start of cycle, t_1: tool enters the workpiece on the first cycle, t_2: tool enters the workpiece on the second cycle, t_3: tool reaches the workpiece surface or end of cycle. All these time points are shown in the Fig. A.1.

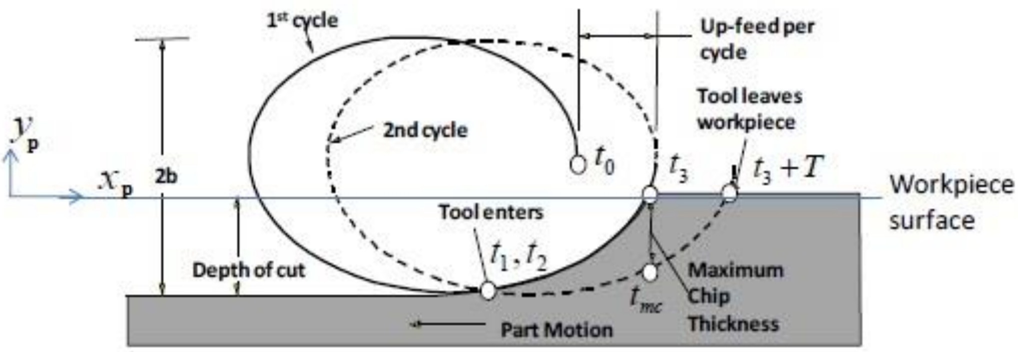

Fig. A.1 Elliptical cutting process and critical time points in part coordinate system

The numerical solution gives the time point equation as follows:

$$t_1 = \frac{\pi}{\omega} + \frac{1}{\omega} cos^{-1}\left(\frac{n.upfc}{2a}\right) \quad \text{(A.3)}$$

$$t_2 = \frac{2\pi}{\omega} - \frac{1}{\omega} cos^{-1}\left(\frac{n.upfc}{2a}\right) \quad \text{(A.4)}$$

Where $n = \left(\frac{a\omega}{(v+a\omega)}\right)$

$$t_3 = \begin{cases} T + \frac{1}{\omega} arcsin\left(\frac{DoC}{b} - 1\right) & if\ b > DoC \\ T & if\ b < DoC \end{cases} \quad \text{(A.5)}$$

Contact time: $(t_3 - t_1)$

r_{up} is the ratio of sliding distance to upfeed per cycle, when multiplied by to total cutting distance, gives the total distance over which the tool is in contact with the workpiece:

$$r_{up} = \frac{d_s}{ufpc} \quad \text{(A.6)}$$

The average wear rate is determined by integrating the instantaneous wear rate for one steady state vibration cycle only over the contact time, but dividing this value by the total cycle period:

$$\left(\frac{dW}{dt}\right)_{Avg} = \frac{1}{T_{Total}}\left(\int_{t_1}^{t_3} \frac{dW}{dt} dt\right) \quad \text{(A.7)}$$

Wear per machining distance is calculated using the following:

$$\left(\frac{dW}{ds}\right)_{Mach} = \frac{1}{v_{wkpc}}\left(\frac{dW}{dt}\right)_{Avg} \quad \text{(A.8)}$$

Where ‘Mach’ shows tool wear over Machining distance and ‘Avg.’ shows average wear value.

ii. Absolute and relative parameters

EVAM wear results may be compared to the conventional machining results using absolute (v_{wkpc}, machining distance, and depth of cut) or relative (v_{rel}, sliding distance, and max uncut chip thickness) terms. While absolute terms represent to true function of EVAM in making a part, relative terms are more appropriate for modeling purposes [26]. Two parameters relate relative to absolute terms: horizontal speed ratio (HSR = $v_{wkpc}/a\omega$) relates absolute to relative velocities, and sliding distance per upfeed ratio (r_{up}) can be multiplied by total machining distance to determine the total contact or rubbing distance between the tool and workpiece.

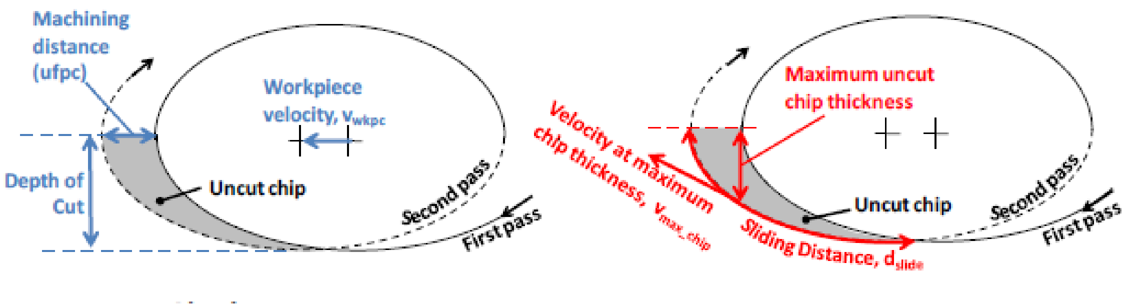

Fig. A.2 Absolute and relative cutting parameters in elliptical cutting process

Wear per sliding distance is determined by dividing $(dW/ds)_{mach}$ in Equation (7) by sliding distance per upfeed ratio:

$$\left(\frac{dW}{ds}\right)_{slide} = \frac{upfc}{d_s}\left(\frac{dW}{ds}\right)_{Mach} = \frac{1}{r_{up}}\left(\frac{dW}{ds}\right)_{Mach} \tag{A.9}$$

The equation 7 can be further described as:

$$\left(\frac{\mathrm{dW}}{\mathrm{ds}}\right)_{\mathrm{slide}} = \frac{1}{\mathrm{t_{contact}} \times \mathrm{v_s}} \int_{\mathrm{t_1}}^{\mathrm{t_3}} \mathrm{A} \times \mathrm{e}^{\frac{-\mathrm{E_a}}{\mathrm{RT}}} \mathrm{dt} \tag{A.10}$$

Appendix B

i. Literature Cutting forces obtained from experiments

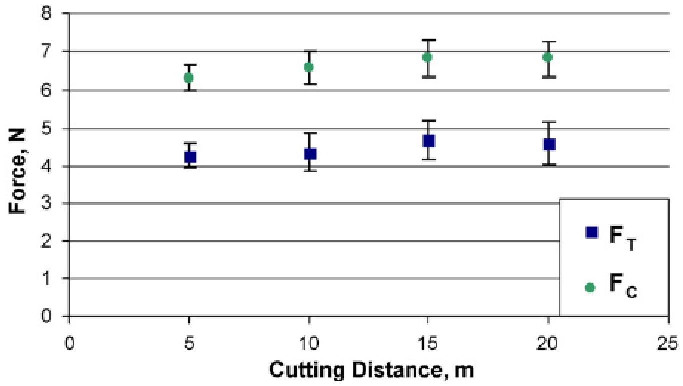

Fig. B.1 Forces Literature Values for Conventional cutting [48]

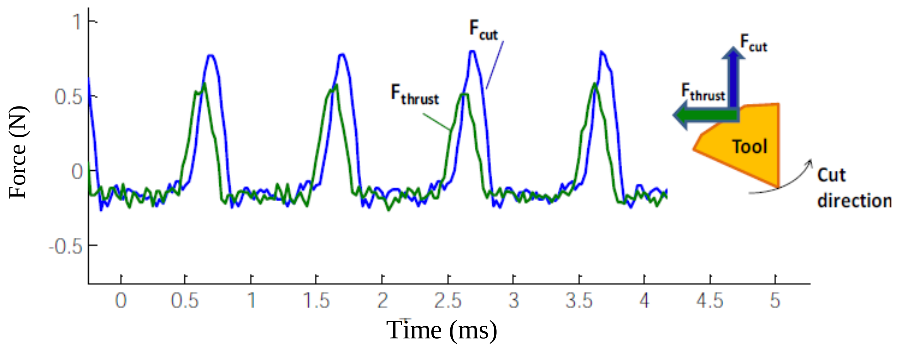

Fig. B.2 Cutting and thrust forces in experimental setup for cutting parameters: DOC: 2 micron, frequency: 1 KHz, ellipse amplitude: 11×2 micron [26]

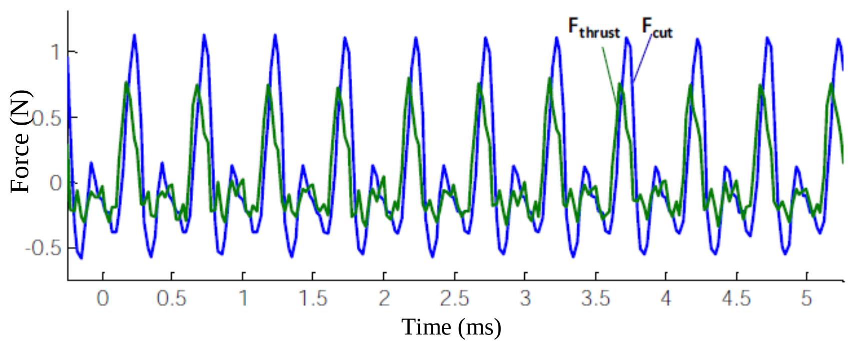

Fig. B.3 Cutting and thrust forces in experimental setup for cutting parameters: DOC: 2 micron, frequency: 2 KHz, ellipse amplitude: 11×2 micron [26]